Commun Nonlinear Sci Numer Simulat 139 (2024) 108265

Contents lists available at ScienceDirect

Communications in Nonlinear Science and Numerical Simulation

journal homepage: www.elsevier.com/locate/cnsns

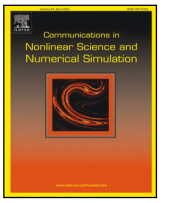

Research paper

Multiple transmission routes in nosocomial bacterial infections — A modeling study

Ziqiang Cheng [a], Hengmin Jia [b,1], Jian Sun [c], Yueguo Wang [c], Shusheng Zhou [c], Kui Jin [c], Mengping Zhang [d], Jin Wang [e,*]

[a] School of Mathematics, Hefei University of Technology, Hefei, Anhui 230009, China
[b] Department of Infection Control, The First Affiliated Hospital of USTC, Division of Life Sciences and Medicine, University of Science and Technology of China, Hefei, Anhui 230001, China
[c] Department of Emergency Medicine, The First Affiliated Hospital of USTC, Division of Life Sciences and Medicine, University of Science and Technology of China, Hefei, Anhui 230001, China
[d] School of Mathematical Sciences, University of Science and Technology of China, Hefei, Anhui 230026, China
[e] Department of Mathematics, University of Tennessee at Chattanooga, Chattanooga, TN 37403, USA

ARTICLE INFO

Keywords:
Bacterial infection
Antibiotic resistance
Mathematical modeling

ABSTRACT

In this paper, we propose a new mathematical model to investigate nosocomial infections caused by both antibiotic-sensitive and antibiotic-resistant bacteria. A focus of our modeling study is the presence of multiple transmission pathways, including the primary infection, co-infection, and re-infection from each type of bacteria, and their interplay with each other in the process of disease spread. We calibrate this model to clinical data and quantify the effects of each transmission route in the epidemic development and evolution. Our data fitting and numerical simulation results indicate that resistant bacteria play a more significant role than sensitive bacteria in shaping the hospital epidemics in our study, highlighting the importance of effective prevention and intervention strategies for antibiotic-resistant bacteria. We also find that the primary infection and re-infection have a larger impact than the co-infection on the short-term and long-term progression of the epidemics.

1. Introduction

Nosocomial infections, which are typically not present at the time of hospital admission but acquired during the process of receiving medical care, represent a significant threat to public health. Particularly, the emergence of drug-resistant bacterial strains in healthcare-associated infections has become an increasingly important issue in hospital settings. In the year of 2019 alone, an estimated 4.95 million deaths occurred that were associated with nosocomial bacterial resistance [1].

Bacteria may develop defense mechanisms against antibiotics through both horizontal gene transfer (i.e., acquisition of new genetic material from another source) and vertical gene transfer (i.e., biological mutation and natural selection). The presence of drug-resistant bacteria leads to treatment failures, significantly wasting medical resources and imposing a heavy burden on both the patients and the healthcare system. Antimicrobial-resistant bacteria can be transmitted in hospitals through the contaminated environment (air, surfaces, liquids, etc.) and through the direct contact between patients and/or health professionals. The prevalence of drug-resistant bacteria in critically ill patients is particularly high, especially among those who have prolonged hospital stays,

* Corresponding author.
E-mail addresses: kuijin@ustc.edu.cn (K. Jin), jin-wang02@utc.edu (J. Wang).
[1] Co-first author.

https://doi.org/10.1016/j.cnsns.2024.108265
Received 7 May 2024; Received in revised form 6 August 2024; Accepted 8 August 2024
Available online 10 August 2024

who are on mechanical ventilation, and who have long-term central venous catheters and urinary catheters in place [2]. Despite tremendous prevention and intervention efforts, clinical burden and mortality attributable to antimicrobial resistance are projected to continuously increase, potentially causing as many as 10 million extra human deaths per year by 2050 [3]. Challenges related to the control of hospital infections and antibiotic resistance are also extensively discussed in [4–6].

As a means of theoretical investigation, many computational models have been proposed to study the complex mechanisms of antibiotic resistance and to help design effective control strategies [7,8]. Particularly, compartmental models have been extensively used [9], following the standard epidemic modeling approach based on systems of differential equations [10–14]. Austin and Anderson [15] published simple mathematical models stemming from the law of mass action to describe the in-host dynamics of antibiotic treatment and the spread of antibiotic-resistant bacteria in intensive care settings as well as between hospitals. Techitnutsarut and Chamchod [16] developed a mathematical model for the within-host behavior of bacterial resistance, incorporating the interaction between sensitive and resistant bacteria. Webb et al. [17] proposed a multi-level model, involving both the bacterial population at the single host level and the patient population at the hospital level, to analyze the dynamic elements of resistant and non-resistant bacterial strains in hospital settings. Related compartmental models also include [18,19] and many others. In addition, stochastic models have been published to study hospital infections involving a small number of patients [20–22]. Among these, Wang and Xiao [22] constructed a stochastic model with direct and indirect bacterial transmission pathways and found that isolating newly admitted patients was the most effective way to reduce bacterial infections. Furthermore, statistical methods have also been commonly used to analyze time series data and make inferences in hospital epidemiology [23–27].

Although significant progress has been made through these modeling studies, several important questions concerned with nosocomial infections and antibiotic-resistant bacteria have not been adequately addressed. For example, how to represent the interaction between resistant and non-resistant (i.e., sensitive) bacteria that may lead to co-infection and re-infection? What are the roles played by the primary infection and secondary infection in shaping a bacterial epidemic in a hospital? How to characterize and quantify the importance of these different transmission routes?

The present paper aims to address these questions by formulating a new compartmental model that incorporates multiple transmission routes relevant to nosocomial bacterial infections. Our model, which describes the complex interaction between resistant and sensitive bacteria and the interplay between primary and secondary infections, will quantify the relative importance of each transmission route in order to inform policy development and infection management. To validate our model, we will use data collected from the intensive care unit (ICU) of the First Affiliated Hospital of the University of Science and Technology of China (FHUSTC), with a focus on drug-resistant *Acinetobacter baumannii* in this study. *Acinetobacter baumannii* is one of the most common drug-resistant bacteria in clinical settings, capable of spreading through multiple transmission routes that include primary infection, co-infection, and re-infection. It can cause infections in the bloodstream, lungs, and urinary tract, severely impacting patient outcomes [2].

ICU patients in general are those that suffer most from infections due to their existing (chronic/emergent) medical conditions that typically compromise their immune functions, and due to the high colonization prevalence of drug-resistant pathogens in the ICUs [28,29]. In an international survey, it was found that 54% of ICU patients overall, and 60% of those in Asia and the Middle East, had suspected or proven infections, with high prevalence of antibiotic resistance and substantial risk of in-hospital mortality [30]. Hence, effective prevention and intervention for antibiotic-resistant bacterial infections are extremely important for the management of ICUs, whose patients represent the most vulnerable population, and can potentially save lives. FHUSTC, with more than 5000 beds, is the leading hospital in Anhui Province of China and one of the largest hospitals in the entire country. Bacterial infections, particularly those caused by antibiotic-resistant *Acinetobacter baumannii*, have been persistent in the ICU of FHUSTC. We have collected data from the ICU of FHUSTC for years 2022 and 2023 which will be used to calibrate and validate our mathematical model.

The remainder of this paper is organized as follows. The mathematical formulation of our bacterial infection model is described in Section 2. Computational results, including parameter estimates through data fitting, numerical tests relevant to short- and long-term dynamics, and simulation studies based on parameter variation, are presented in Section 3. The paper is concluded with some discussion in Section 4.

2. Mathematical formulation

We consider two types of bacteria that cause nosocomial infections: one is sensitive to antibiotic treatment, referred to as type A in our modeling study, and the other is resistant to antibiotic treatment, referred to as type B. Our classifications of type A and type B are broad, and each of them may contain several subtypes of bacteria.

We will examine the transmission dynamics of both types of bacteria as well as their interplay in the spread of the infection, and will use data from the ICU of FHUSTC to validate our model. Our empirical observations showed that both type A and type B bacteria could lead to a significant number of primary infections and that type B infection may protect patients from co-infection with type A bacteria, but patients with type A infection may still be at risk for co-infection with type B bacteria. Our clinical data also showed that recovery from infection would protect patients from re-infection with bacteria of the same type but not the different type. Specifically, we will incorporate the following observations into our model formulation:

- When a patient is infected with type A bacteria, there is a possibility of co-infection with type B bacteria.
- When a patient is infected with type B bacteria, the probability of co-infection with type A bacteria is almost 0.
- After a patient recovers from type A infection, the probability of re-infection with type A bacteria is almost 0.

- After a patient recovers from type A infection, the probability of re-infection with type B bacteria is the same as that of a person who has not been infected by type A bacteria.
- After a patient recovers from type B infection, the probability of re-infection with type B bacteria is almost 0.
- After a patient recovers from type B infection, the probability of re-infection with type A bacteria is the same as that of a person who has not been infected by type B bacteria.

We divide the ICU patient population into nine compartments containing, respectively, susceptible individuals (denoted by S), individuals with primary infection from type A bacteria (denoted by I_0), individuals with primary infection from type B bacteria (denoted by I_1), individuals with co-infection from both types of bacteria (denoted by I_{01}), individuals with re-infection from type A bacteria (denoted by $\tilde{I}_0$), individuals with re-infection from type B bacteria (denoted by $\tilde{I}_1$), recovered individuals from primary type A infection (denoted by R_0), recovered individuals from primary type B infection (denoted by R_1), and recovered individuals from infection with both types of bacteria (denoted by R_{01}). Our model includes the following transmission routes:

- Primary infection with type A bacteria: $S \to I_0 \to R_0$
- Primary infection with type B bacteria: $S \to I_1 \to R_1$
- Co-infection with both types of bacteria: $S \to I_0 \to I_{01} \to R_{01}$
- Re-infection with type A bacteria: $R_1 \to \tilde{I}_0 \to R_{01}$
- Re-infection with type B bacteria: $R_0 \to \tilde{I}_1 \to R_{01}$

Mathematically, the model is described by the following differential equations:

$$\begin{aligned}
\frac{dS}{dt} &= \Gamma - \beta_0 S(I_0 + \tilde{I}_0 + I_{01}) - \beta_1 S(I_1 + \tilde{I}_1 + I_{01}) - \mu S,\\
\frac{dI_0}{dt} &= \beta_0 S(I_0 + \tilde{I}_0 + I_{01}) - \beta_{01} I_0(I_1 + \tilde{I}_1 + I_{01}) - (\gamma_0 + \omega) I_0,\\
\frac{dI_1}{dt} &= \beta_1 S(I_1 + \tilde{I}_1 + I_{01}) - (\gamma_1 + \omega) I_1,\\
\frac{dI_{01}}{dt} &= \beta_{01} I_0(I_1 + \tilde{I}_1 + I_{01}) - (\gamma_{01} + \omega) I_{01},\\
\frac{d\tilde{I}_0}{dt} &= \beta_0 R_1(I_0 + \tilde{I}_0 + I_{01}) - (\gamma_0 + \omega)\tilde{I}_0,\\
\frac{d\tilde{I}_1}{dt} &= \beta_1 R_0(I_1 + \tilde{I}_1 + I_{01}) - (\gamma_1 + \omega)\tilde{I}_1,\\
\frac{dR_0}{dt} &= \gamma_0 I_0 - \beta_1 R_0(I_1 + \tilde{I}_1 + I_{01}) - \mu R_0,\\
\frac{dR_1}{dt} &= \gamma_1 I_1 - \beta_0 R_1(I_0 + \tilde{I}_0 + I_{01}) - \mu R_1,\\
\frac{dR_{01}}{dt} &= \gamma_{01} I_{01} + \gamma_0 \tilde{I}_0 + \gamma_1 \tilde{I}_1 - \mu R_{01}.
\end{aligned} \tag{2.1}$$

Patients who need intensive care are admitted to the ICU at the influx rate Γ. We assume that all these patients are susceptible to the bacterial infection under our consideration. Susceptible individuals contract type A and type B bacteria with the primary infection rates β_0 and β_1, respectively. Individuals with type A infection may contract type B bacteria at the rate β_{01} and enter the co-infection class, who may spread both types of bacteria. Individuals with type A infection, type B infection, and co-infection recover at rates γ_0, γ_1, and γ_{01}, respectively. Recovered individuals from type A infection may undergo re-infection with type B bacteria at the rate β_1, and recovered individuals from type B infection may undergo re-infection with type A bacteria at the rate β_0, whereas recovered individuals who have contracted both types of bacteria are protected from re-infection. In addition, susceptible and recovered individuals may be discharged from the ICU at a rate μ, and infected individuals have a disease-induced mortality rate ω that is assumed to be the same for both types of infections.

3. Numerical study

3.1. Model fitting with clinical data

We have collected patient data from the ICU of FHUSTC in two 9-month periods: 1/1/2022–9/30/2022 and 1/1/2023–9/30/2023, with 272 days in each period. For both years, the vast majority of antibiotic-resistant infections were caused by *Acinetobacter baumannii*, which will represent the type B bacteria in our model. The antibiotic-sensitive bacteria related to our data include *Escherichia coli*, *Staphylococcus aureus*, *Streptococcus pneumoniae*, *Klebsiella pneumoniae*, etc., and they will be aggregated into the type A bacteria in our model. The data include the number of patients entering the ICU each day, the number of new cases for type A and type B infections on a daily basis, and the duration of infection and the length of stay for each patient in the ICU.

Our data show that the average recovery period for type A infection, caused by sensitive bacteria, is about 6 days, which leads to $\gamma_0 = 1/6$ per day. In contrast, type B infection, caused by resistant bacteria, typically lasts longer and the average recovery period is about 10.5 days. We thus take $\gamma_1 = 1/10.5$ per day and $\gamma_{01} = 1/10.5$ per day. Our data also indicate that the average length of

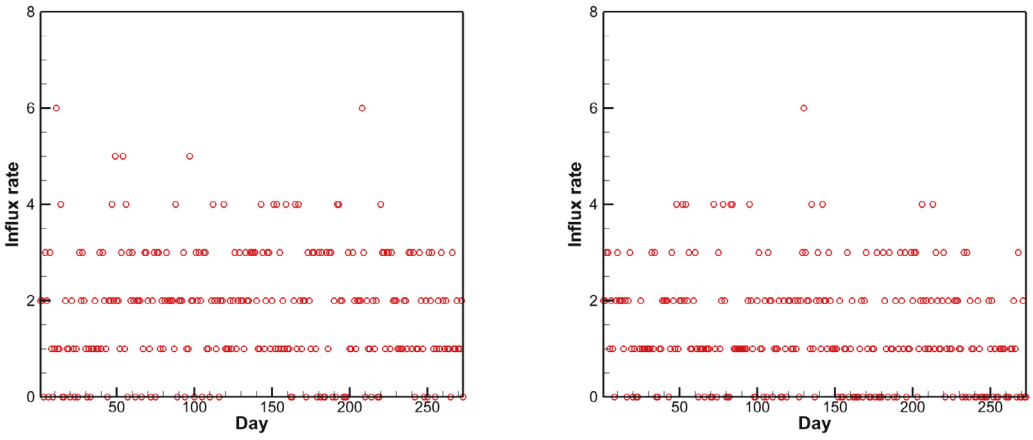

(a) 1/1/2022–9/30/2022 (b) 1/1/2023–9/30/2023

Fig. 1. Data for the influx rate Γ in 2022 and 2023.

Table 1
Parameters in model (2.1) and their values.

Parameter	Description	Value
Γ	Influx rate	Varied
γ_0	Recovery rate of type A bacterial infection	1/6 per day
γ_1	Recovery rate of type B bacterial infection	1/10.5 per day
γ_{01}	Recovery rate of co-infection	1/10.5 per day
μ	Discharge rate	1/5 per day
β_0	Primary infection and re-infection rate of type A bacteria	Fitted by data
β_1	Primary infection and re-infection rate of type B bacteria	Fitted by data
β_{01}	Co-infection rate	Fitted by data
ω	Infection-induced mortality rate	Fitted by data

stay in the ICU for patients free of infection (including both susceptible and recovered individuals) is about 5 days. We thus set the discharge rate as $\mu = 1/5$ per day. Additionally, since we have detailed data for the daily number of people entering the ICU, we use that data to determine the influx rate Γ which is changing from day to day (see Fig. 1). For both the 9-month periods in 2022 and 2023, Γ varied between 0 to 6 persons per day. These parameters and their values are listed in Table 1.

The other four model parameters, including the primary infection rates β_0 and β_1, the co-infection rate β_{01}, and the infection-induced death rate ω, cannot be directly observed from our collected data. Instead, we will estimate their values through model calibration based on data fitting. In what follows, we will focus on the 9-month data in 2023 and present the fitting and simulation results. We will briefly discuss the results for the 9-month data in 2022 in Section 3.4.

We fit our model to the daily reported new cases for both type A and type B infections. Our error function is defined as follows

$$\sum_{i=1}^{272} \left\{ \left[X_A(i) - Y_A(i)\right]^2 + W^2 \left[X_B(i) - Y_B(i)\right]^2 \right\}, \tag{3.1}$$

where $Y_A(i)$ and $Y_B(i)$ denote, respectively, the reported number of new cases from the collected data for type A and type B infections on the ith day, and $X_A(i) = \beta_0(S + R_1)(I_0 + \tilde{I}_0 + I_{01})$ and $X_B(i) = \beta_1(S + R_0)(I_1 + \tilde{I}_1 + I_{01}) + \beta_{01} I_0 (I_1 + \tilde{I}_1 + I_{01})$ represent, respectively, our model predictions for the number of type A and type B new infections on the ith day, $1 \le i \le 272$. Thus, the error function is a summation of errors for each day in the 9-month period (272 days), with each term being a square sum of the error associated with type A new cases and that associated with type B new cases. The parameter W is a scaling factor introduced to balance the two errors, which may be taken as the ratio of the average number of new type A infections and that of type B infections. The least squares method is applied to minimize the error function and estimate the four parameters β_0, β_1, β_{01}, and ω.

The fitted parameter values and their 95% confidence intervals are presented in Table 2. We observe that the two primary infection rates (β_0 and β_1) are at the same order, whereas the co-infection rate (β_{01}) is one order lower. Since β_0 and β_1 also represent the re-infection rates, the results indicate that the primary infection and re-infection play a more important role than the co-infection. Fig. 2 shows the numerical results for the numbers of new cases and cumulative cases caused by type A and type B bacteria, based on data fitting. We observe reasonably good agreement between our simulation results and the reported data.

When the influx rate can be treated as a constant (e.g., approximated by its time-averaged value), we may conveniently quantify the risk of infection using the basic reproduction number associated with the autonomous system. Based on the fitting results, we

Table 2
Fitted parameter values and confidence intervals based on data in 2023.

Parameter	Fitted value	95% Confidence interval
β_0	2.7316E−02	(2.5704E−02, 2.8928E−02)
β_1	1.5825E−02	(1.5824E−02, 1.5825E−02)
β_{01}	3.5193E−03	(1.9075E−03, 5.1312E−03)
ω	1.9162E−03	(1.9141E−03, 1.9182E−03)

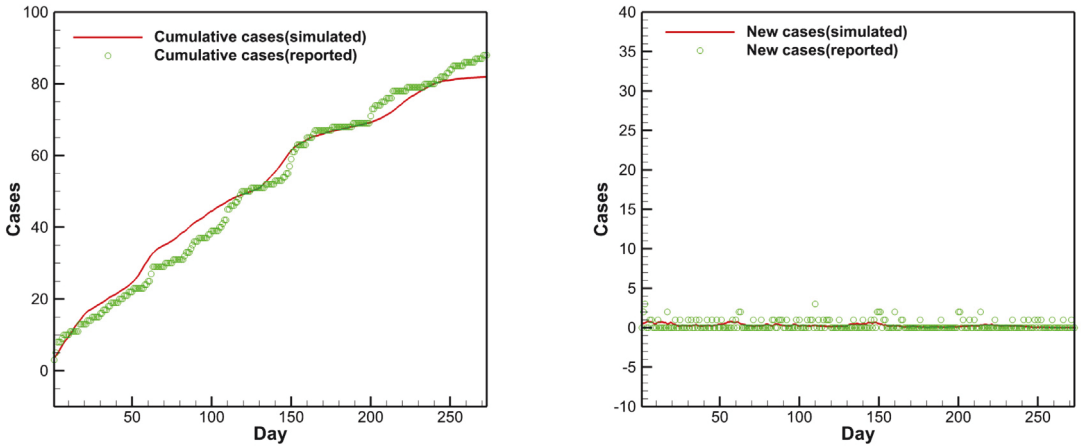

(a) Type A bacterial infection

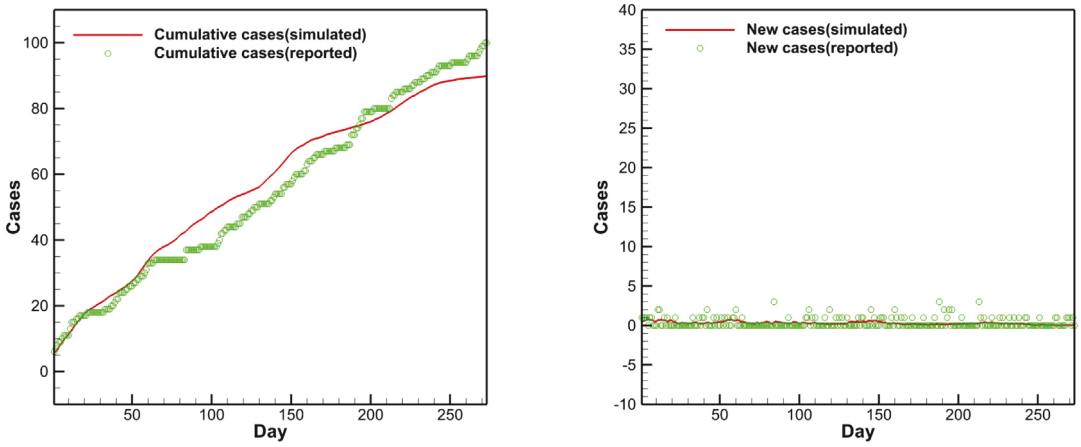

(b) Type B bacterial infection

Fig. 2. Numerical results for the number of cumulative cases and the number of new cases caused by type A and type B bacteria based on the 272-day data in 2023.

may estimate the basic reproduction number using the formula derived in Appendix A, Eq. (A.2):

$$\mathscr{R}_0 = \max(\mathscr{R}_{00}, \mathscr{R}_{01}) = \max(1.1069, 1.1127) = 1.1127, \tag{3.2}$$

where $\mathscr{R}_{00}$ and $\mathscr{R}_{01}$ represent the infection risk due to type A and type B bacteria, respectively. Since $\mathscr{R}_0 > 1$, the indication is that the infection would persist. Meanwhile, since $\mathscr{R}_0 = \mathscr{R}_{01} > \mathscr{R}_{00}$, it shows that resistant bacteria (type B) are the stronger force for the persistence of the nosocomial infection.

Additionally, a sensitivity analysis for the model parameters is conducted in Appendix B. We note, in particular, that the two primary infection and re-infection rates β_0 and β_1 are highly sensitive to both the state variables and the basic reproduction number.

3.2. Impact of different transmission routes

A distinct feature of our model is that it incorporates multiple transmission routes in the spread of bacterial infection in the ICU. Specifically, the variables I_0 and I_1 represent the result of the primary infection from the two types of bacteria, I_{01} represents that of co-infection, and $\tilde{I}_0$ and $\tilde{I}_1$ represent that of re-infection. The total number of active cases at any time is then given by $I_0 + I_1 + I_{01} + \tilde{I}_0 + \tilde{I}_1$.

In order to quantify the impact of these different transmission routes, we have conducted a set of hypothetical tests, presented in Fig. 3. Each test is concerned with one single transmission pathway, where we remove that specific transmission route and compare the result with the original scenario in terms of the number of active infections. First, we remove the primary transmission caused by type A bacteria by setting $I_0 = 0$, while keeping all other components of the model. We then run this reduced model and generate the curve for the total number of active cases, and plot this curve in Fig. 3(a) together with the result based on the original model. We observe a significant reduction in the number of active cases, without the contribution from type A bacteria. Second, we remove the primary transmission caused by type B bacteria by setting $I_1 = 0$, and then run the reduced model to generate the curve shown in Fig. 3(b). Compared to the result in panel (a), we observe an even stronger reduction of the active infection level in panel (b), indicating again that type B (i.e., resistant) bacteria may play a more important role than type A (i.e., sensitive) bacteria in shaping the hospital epidemics. Third, Fig. 3(c) shows the result by removing the co-infection ($I_{01} = 0$), where it can be seen that the impact of co-infection is weaker than that of the primary infection. Additionally, panels (d), (e) and (f) show the results by removing the type A re-infection ($\tilde{I}_0 = 0$), type B re-infection ($\tilde{I}_1 = 0$), and re-infection from both types ($\tilde{I}_0 = \tilde{I}_1 = 0$), respectively. We observe that the effects of re-infection are somewhere between those of primary infection and co-infection.

Next, we have also studied the impact of each transmission route on the number of cumulative cases. Figs. 4 and 5 display the results for the cumulative cases due to type A and type B bacteria, respectively. For each figure, the cumulative cases include all the infected cases from the primary infection, co-infection, and re-infection that are caused by one of the two types of bacteria. In Fig. 4, we observe that type A primary infection (panel a) plays a dominant role in shaping the cumulative cases associated with type A bacteria, followed by type A re-infection (panel d) and co-infection (panel c). In contract, type B primary infection (panel b) and re-infection (panel e) play relatively minor roles in this regard. Fig. 5 shows the opposite, where type B primary infection (panel b) plays a dominant role in shaping the cumulative cases associated with type B bacteria, followed by type B re-infection (panel e), while type A primary infection (panel a) and re-infection (panel d) play relatively minor roles.

Furthermore, we have conducted numerical simulation for the long-term dynamics of the model which can be compared to the mathematical results presented in Appendix A. To that end, we have replaced the variable influx rate Γ by its time-averaged value so that system (2.1) becomes autonomous. We then run the simulation for 2000 days, sufficiently long to quantify the dynamical behavior at the steady state. Our analysis in Appendix A shows that the autonomous system has a disease-free equilibrium in the form of $X^0 = (S^0, 0, 0, 0, 0, 0, 0, 0, 0)$, a type A boundary equilibrium in the form of $X^A = (S^A, I_0^A, 0, 0, 0, 0, R_0^A, 0, 0)$, a type B boundary equilibrium in the form of $X^B = (S^B, 0, I_1^B, 0, 0, 0, 0, R_1^B, 0)$, and a positive endemic equilibrium in the form of $X^* = (S^*, I_0^*, I_1^*, I_{01}^*, \tilde{I}_0^*, \tilde{I}_1^*, R_0^*, R_1^*, R_{01}^*) > 0$. Their specific values under our data setting are given in Eq. (A.6). The numerical solution for this system converges to the endemic equilibrium X^* where the total number of active infections is $0.8018 + 1.5549 + 0.0516 + 0.1013 + 0.1695 = 2.6791$, plotted as the red curve in each panel of Fig. 6. This is consistent with the fact that $\mathscr{R}_{00} > 1$ and $\mathscr{R}_{01} > 1$.

Setting $I_0 = 0$ (i.e., removing type A primary infection) in this autonomous system, we obtain a reduced system which has only two equilibria, corresponding to the DFE X^0 and the type B boundary equilibrium X^B of the original system - see the statement (A1) in Appendix A. The numerical solution for the reduced system converges to the boundary equilibrium, shown in panel (a) of Fig. 6, where the total number of active infections is 1.4247 at the equilibrium. Similarly, setting $I_1 = 0$ (i.e., removing type B primary infection) leads to the reduced system whose only two equilibria correspond to the DFE X^0 and the type A boundary equilibrium X^A of the original system - see the statement (A2) in Appendix A. As shown in panel (b) of Fig. 6, the numerical solution converges to an active infection level of 0.7829 associated with the boundary equilibrium. When setting $I_{01} = 0$ (i.e., removing co-infection), the reduced system has four equilibria, the fourth of which is a positive equilibrium X^{01} unique to the reduced system - see the statement (A3) in Appendix A. The numerical solution, shown in panel (c), converges to X^{01} where the total number of active infections is $0.5085 + 1.3027 + 0.0524 + 0.0864 = 1.95$ at the equilibrium. Moreover, panels (d), (e) and (f) display the numerical results by setting $\tilde{I}_0 = 0$ (i.e., removing type A re-infection), $\tilde{I}_1 = 0$ (i.e., removing type B re-infection), and $\tilde{I}_0 = \tilde{I}_1 = 0$ (i.e., removing both types of re-infection), respectively. These are stated in (A4), (A5) and (A6) in Appendix A. In each of these scenarios, the reduced system has four equilibria, including a positive equilibrium which the numerical solution converges to.

Overall, we observe that type B primary infection, caused by the antibiotic-resistant bacteria, has the highest impact on the disease prevalence in the long run by comparing panel (b) with other panels in Fig. 6. This is consistent with the finding from Fig. 3 on the short-term dynamics. Although the observation from Fig. 6 is based on a constant influx rate, qualitatively similar results can be expected for time-dependent Γ; i.e., effective control of resistant bacteria will be critical in order to push the long-term prevalence of hospital infections toward a sufficiently low level.

3.3. Simulation with varied parameters

Based on our data fitting results, we have conducted numerical simulation for a period of 8 weeks immediately following the 9-month fitting period as a means to predict the development and evolution of the epidemic. Meanwhile, we have varied several model parameters in the simulation process so as to explore a range of possible scenarios in the epidemic progression. Specifically,

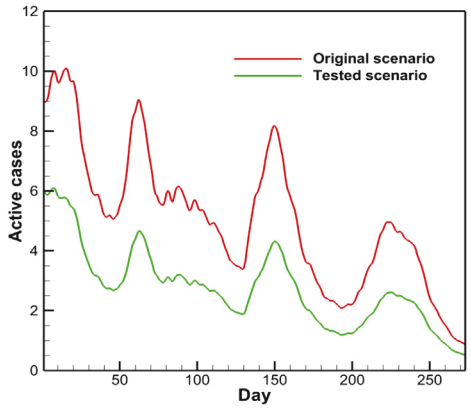

(a) $I_0 = 0$

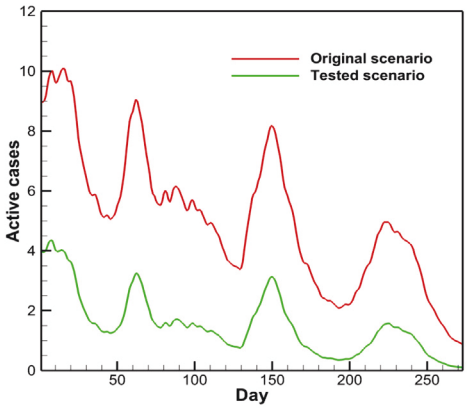

(b) $I_1 = 0$

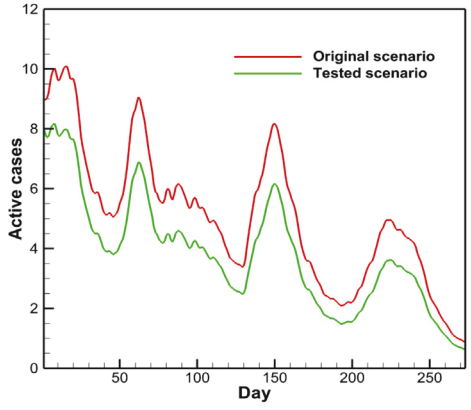

(c) $I_{01} = 0$

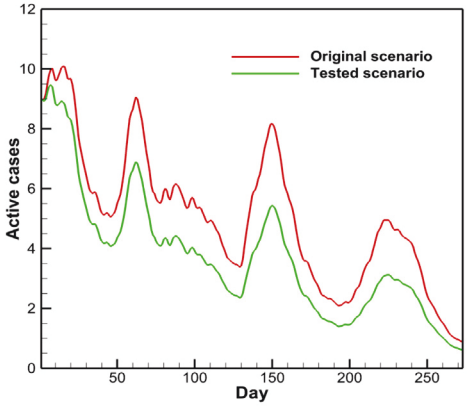

(d) $\tilde{I}_0 = 0$

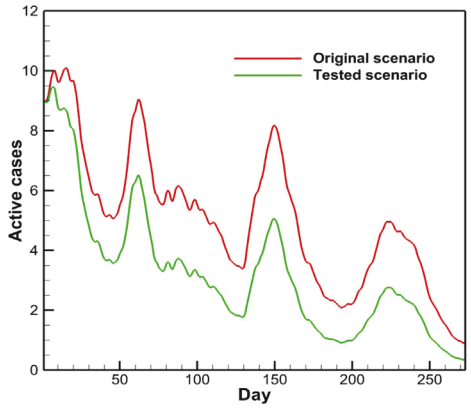

(e) $\tilde{I}_1 = 0$

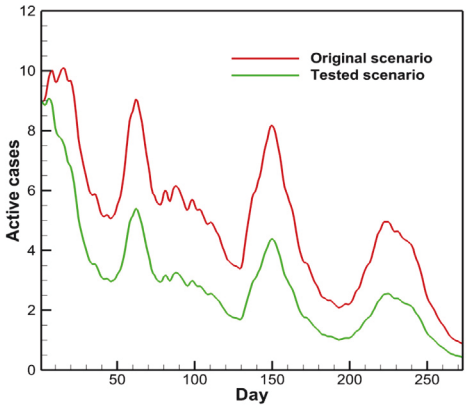

(f) $\tilde{I}_0 = \tilde{I}_1 = 0$

Fig. 3. Impact of different transmission routes on the number of active cases based on data in 2023.

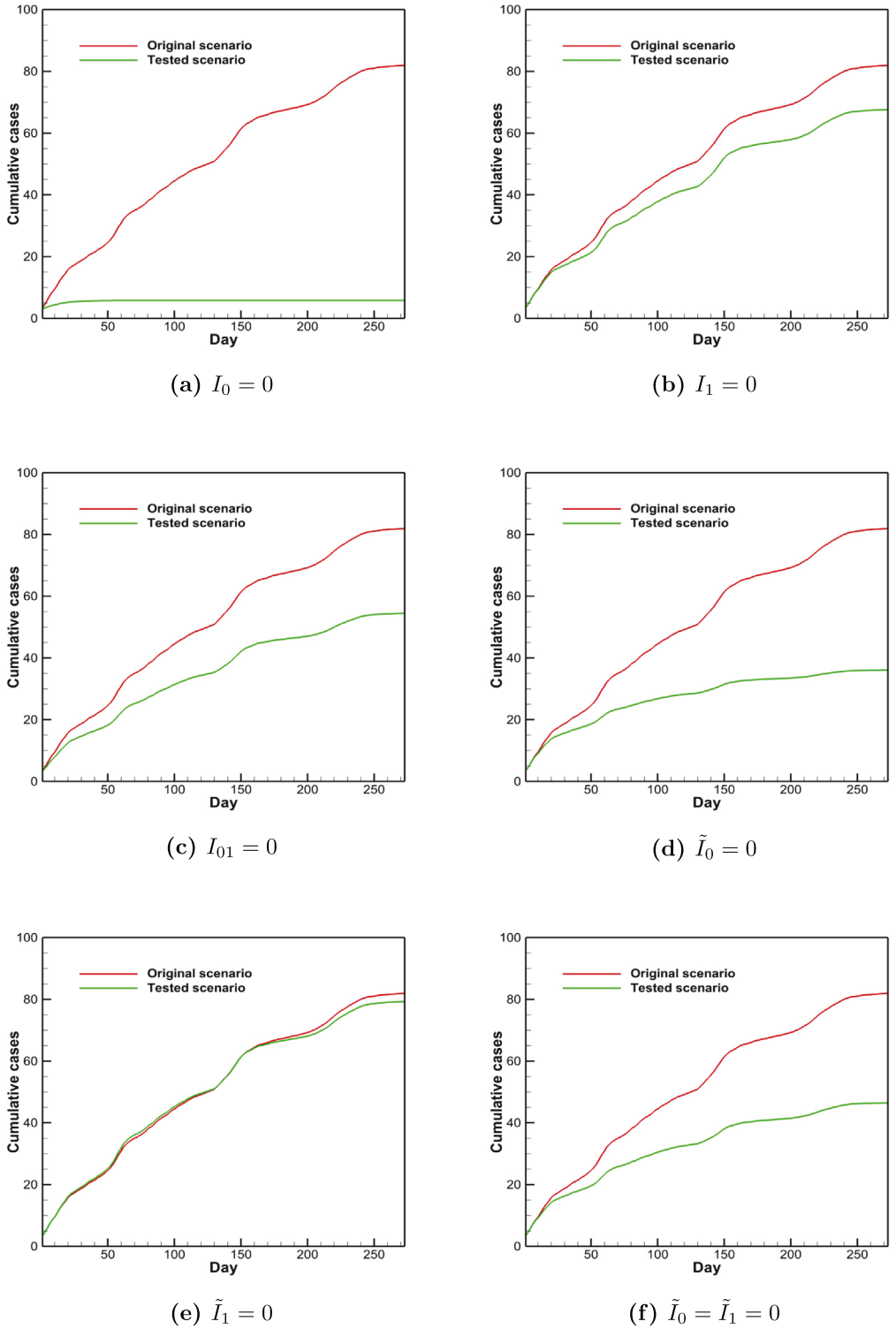

(a) $I_0 = 0$ (b) $I_1 = 0$

(c) $I_{01} = 0$ (d) $\tilde{I}_0 = 0$

(e) $\tilde{I}_1 = 0$ (f) $\tilde{I}_0 = \tilde{I}_1 = 0$

Fig. 4. Impact of different transmission routes on the number of cumulative cases caused by type A bacteria based on data in 2023.

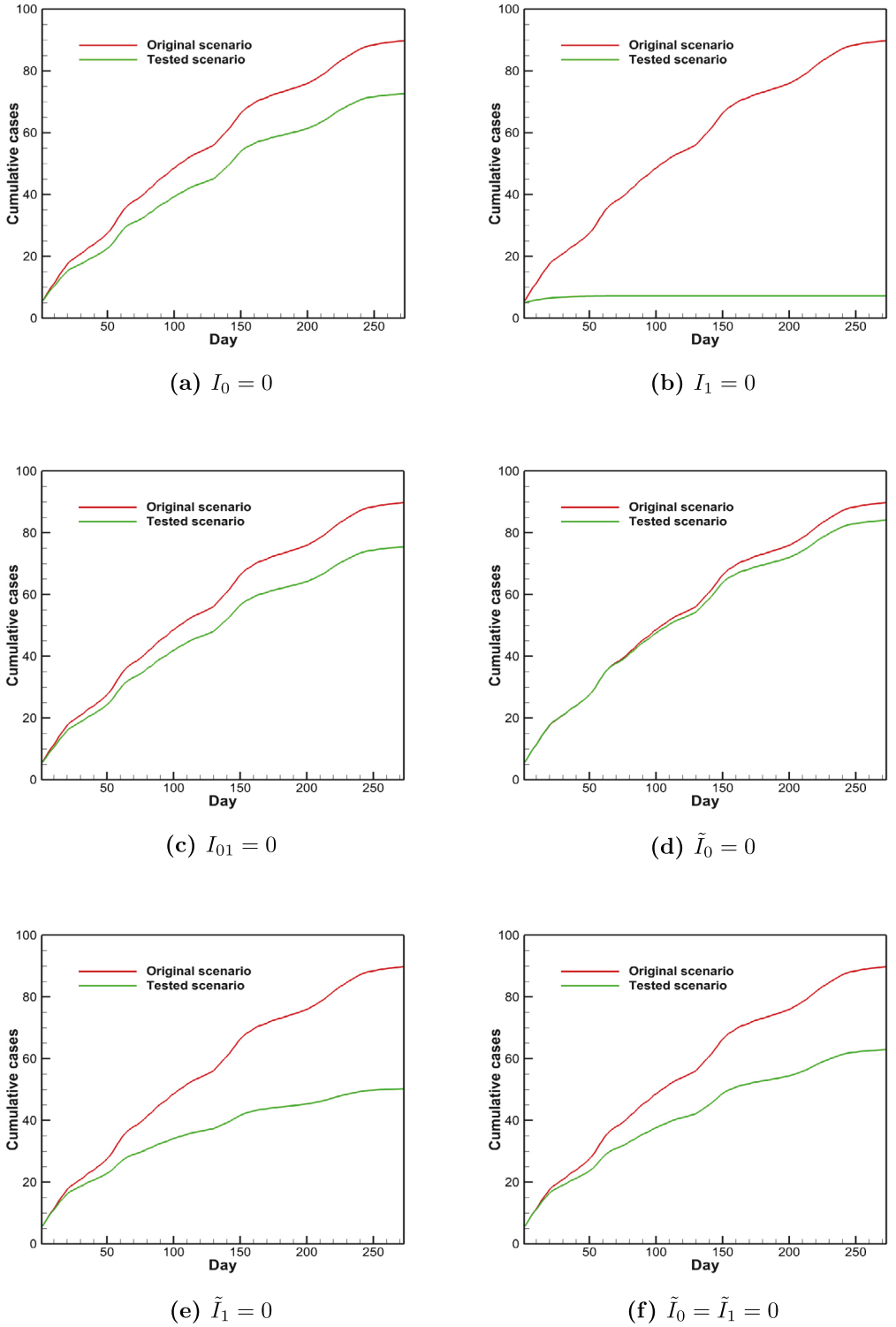

Fig. 5. Impact of different transmission routes on the number of cumulative cases caused by type B bacteria based on data in 2023.

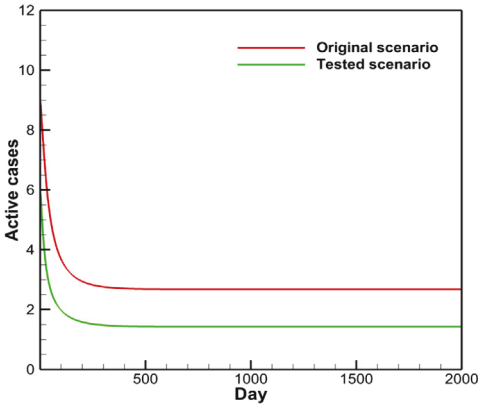

(a) $I_0 = 0$: steady state at 1.4247

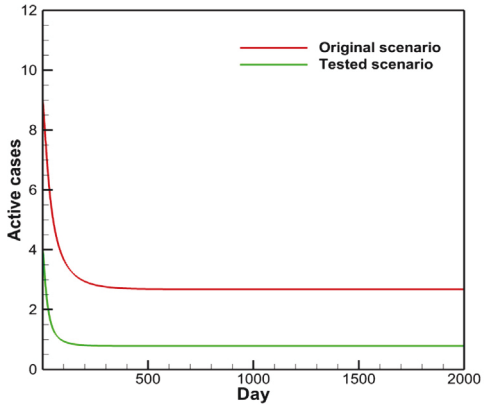

(b) $I_1 = 0$: steady state at 0.7829

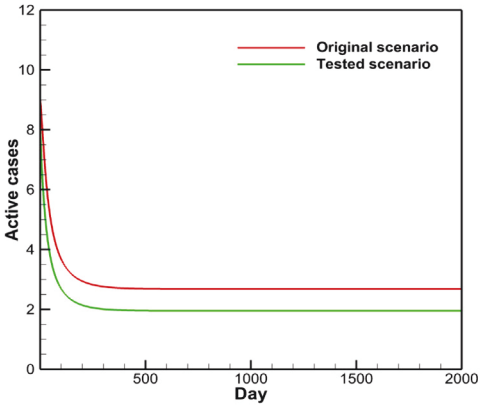

(c) $I_{01} = 0$: steady state at 1.9500

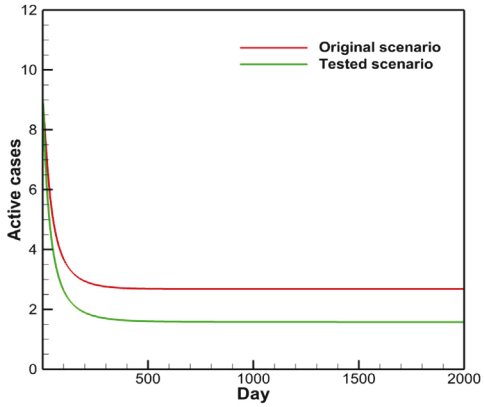

(d) $\tilde{I}_0 = 0$: steady state at 1.5732

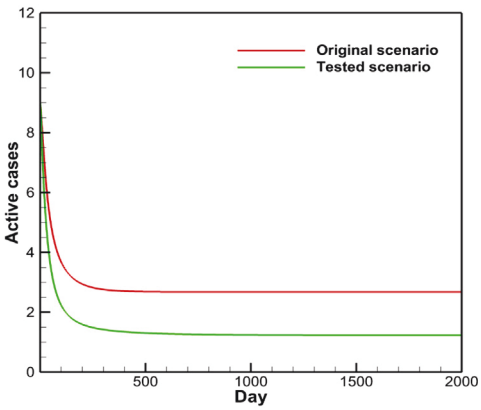

(e) $\tilde{I}_1 = 0$: steady state at 1.2277

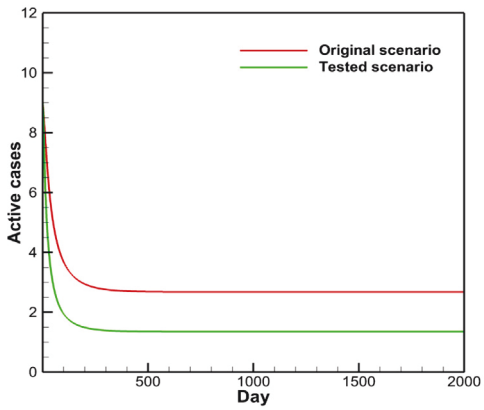

(f) $\tilde{I}_0 = \tilde{I}_1 = 0$: steady state at 1.3447

Fig. 6. Impact of different transmission routes on the long-term progression of the number of active cases. In the original scenario, the solution converges to the steady state at 2.6791. In each tested scenario, the solution converges to a different steady state.

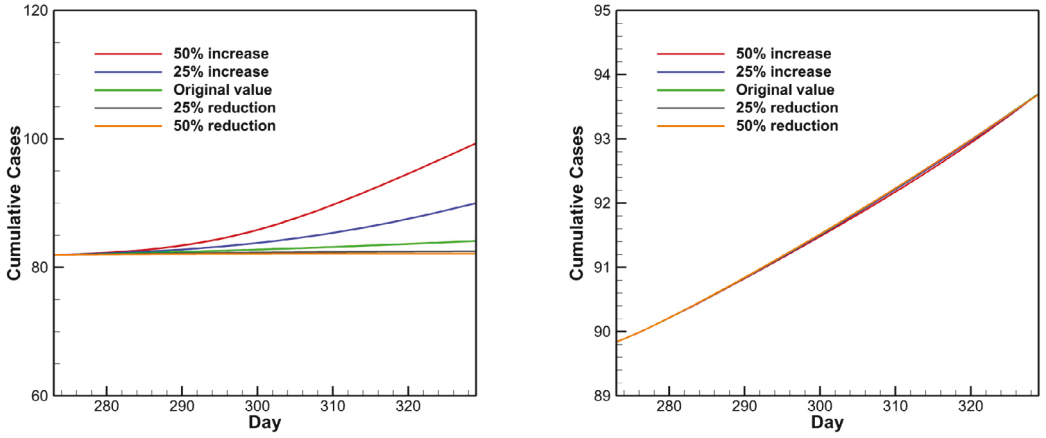

(a) Type A bacterial infection (b) Type B bacterial infection

Fig. 7. Model predictions for the number of cumulative cases in an 8-week period (i.e., from day 273 to day 328) immediately following the 272-day fitting period in 2023, with the type A transmission rate β_0 varied.

we treat the parameter values given in Table 1 as well as those estimated from data fitting (Table 2) as baseline values. We then focus on the three transmission rates (β_0, β_1 and β_{01}) and the three recovery rates (γ_0, γ_1 and γ_{01}). We perturb each one separately by $\pm 25\%$ and $\pm 50\%$ in reference to its base value, while fixing other parameters at their base values. We next run the model and generate the simulation curves for the number of cumulative cases in the 8-week prediction period (i.e., from day 273 to day 328) that immediately follow the 9-month (or, 272-day) fitting period. The numerical solution at the end of the fitting period (i.e., day 272) is used as the initial condition to start the simulation for the prediction period.

The simulation results with variations for the transmission rate β_0 are presented in Fig. 7, where the left and right panels represent the number of cumulative cases associated with type A and type B bacteria, respectively. We clearly observe that, as β_0 is increased by 25% and 50% in reference to its base value, the type A cumulative cases also increase significantly. In contrast, when β_0 is decreased by 25%, the number of type A cumulative cases barely increases throughout the prediction period. A further reduction of β_0 by 50% produces an even lower cumulative infection level, though the improvement appears to be minor. On the other hand, the variation of β_0 has very little impact on the number of type B cumulative cases.

Fig. 8 displays the simulation results with the transmission rate β_1 varied, where panel (b) exhibits a similar pattern as observed in Fig. 7(a). However, unlike what happens in Fig. 7(b), panel (a) of Fig. 8 shows that the variation of β_1 also has a considerable impact on the number of type A cumulative cases through the interplay between the transmission and spread of the two types of bacteria. This result is consistent with what we have observed in Section 3.2 and indicates that reducing the transmission rate of the resistant bacteria can lower the cumulative cases for both type A and type B infections.

Fig. 9 displays the results when the co-infection rate β_{01} is varied, where we observe that this parameter appears to play a minor role for the number of cumulative cases in both type A and type B, and the variation of its values has very minor impact on the prediction outcomes.

Additionally, Figs. 10–12 plot the simulation results when the recovery rates γ_0, γ_1 and γ_{01} are varied, respectively. In general, the value of each recovery rate is inversely correlated to the number of cumulative cases as a faster recovery would shorten the infectious period and reduce the risk of disease spread. We observe that a 25% increase in the type A recovery rate γ_0 would make the curve of the type A cumulative cases almost flat throughout the 8-week period, while a 50% increase would further push the curve down though the difference is barely noticeable; see Fig. 10(a). A similar pattern is clear in Fig. 11(b) for the change of the type B recovery rate γ_1 with respect to the curves of type B cumulative cases. Meanwhile, as shown in Figs. 10(b) and 11(a), the value of γ_1 has a higher impact on the type A cumulative infections than the value of γ_0 does on the type B cumulative infections. Finally, we observe from Fig. 12 that the impact of the co-infection recovery rate γ_{01} is more significant on the type A cumulative cases than that on the type B cumulative cases.

3.4. Fitting and simulation for data in 2022

We acknowledge that the number of infected individuals in our dataset is relatively low, which may give rise to stochastic effects. To confirm that such random effects do not have a major impact on our fitting and simulation results presented in the previous sections for the year of 2023, we have also fitted our model to the 9-month data in 2022 collected from the ICU at FHUSTC. The fitted parameter values and their confidence intervals are presented in Table 3. Meanwhile, numerical results for the numbers of new cases and cumulative cases are plotted in Fig. 13. Based on the data fitting, the basic reproduction number for the autonomous system can be evaluated as

$$\mathscr{R}_0 = \max(\mathscr{R}_{00}, \mathscr{R}_{01}) = \max(1.0040, 0.9792) = 1.0040. \tag{3.3}$$

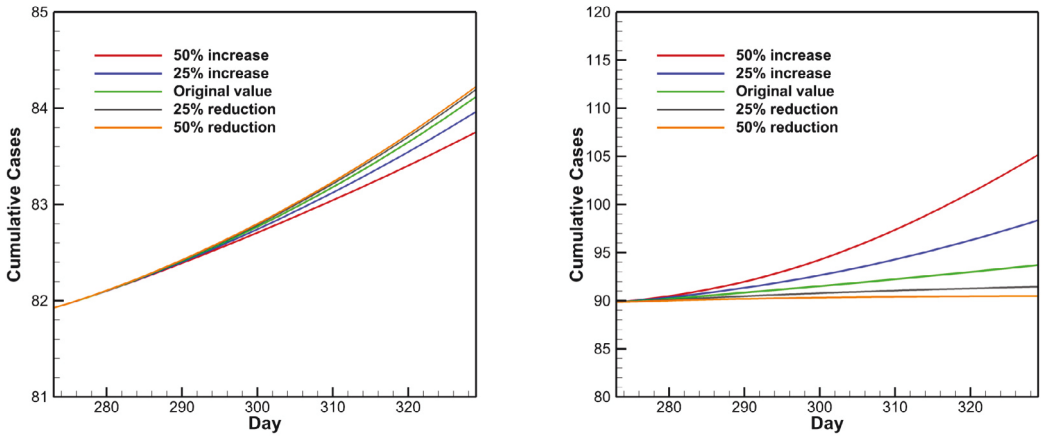

(a) Type A bacterial infection (b) Type B bacterial infection

Fig. 8. Model predictions for the number of cumulative cases in an 8-week period (i.e., from day 273 to day 328) immediately following the 272-day fitting period in 2023, with the type B transmission rate β_1 varied.

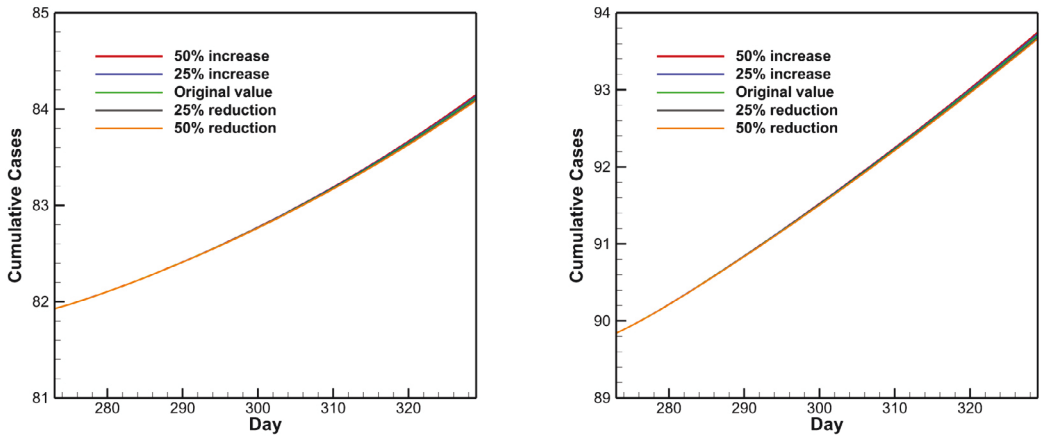

(a) Type A bacterial infection (b) Type B bacterial infection

Fig. 9. Model predictions for the number of cumulative cases in an 8-week period (i.e., from day 273 to day 328) immediately following the 272-day fitting period in 2023, with the co-infection rate β_{01} varied.

Table 3
Fitted parameter values and confidence intervals based on data in 2022.

Parameter	Fitted value	95% Confidence interval
β_0	1.9617E−02	(1.2406E−02, 2.6827E−02)
β_1	1.1242E−02	(5.1804E−03, 1.7303E−02)
β_{01}	7.8415E−03	(0, 2.0510E−02)
ω	6.5349E−03	(0, 4.2839E−02)

We notice that the number of infections (from both type A and type B bacteria) in 2022 is much lower than that in 2023. Correspondingly, the fitted values of the two primary transmission rates β_0 and β_1, which play a dominant role in shaping the epidemic, in the year of 2022 are considerably lower than their counterparts in 2023, leading to a lower basic reproduction number in 2022 than that in 2023. This can be naturally expected, since the first 9 months of 2022 fall into the multi-year period when the dynamic zero-COVID policy was implemented in China [31]. The contact tracing, mass testing, strict sanitation, and extensive quarantine practices in accordance with this policy significantly reduced the population's exposure to pathogens, including not only SARS-CoV-2 but also other infectious agents such as nosocomial bacteria. Consequently, the transmission and spread of bacterial infections in the ICU seemed be effectively suppressed during this period. Such control measures appeared to be especially significant for drug-resistant bacteria as the value of the type B reproduction number $\mathscr{R}_{01}$ falls below unity, based on Eq. (3.3). After the end of

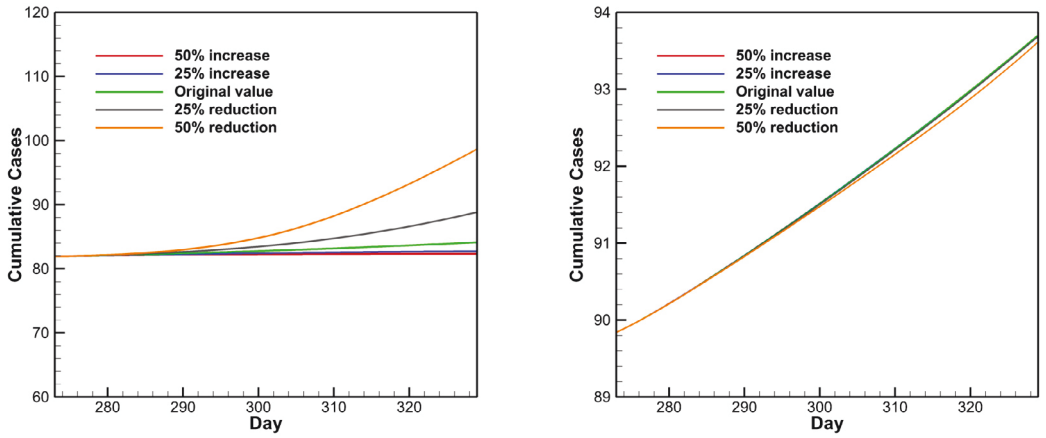

Fig. 10. Model predictions for the number of cumulative cases in an 8-week period (i.e., from day 273 to day 328) immediately following the 272-day fitting period in 2023, with the type A recovery rate γ_0 varied.

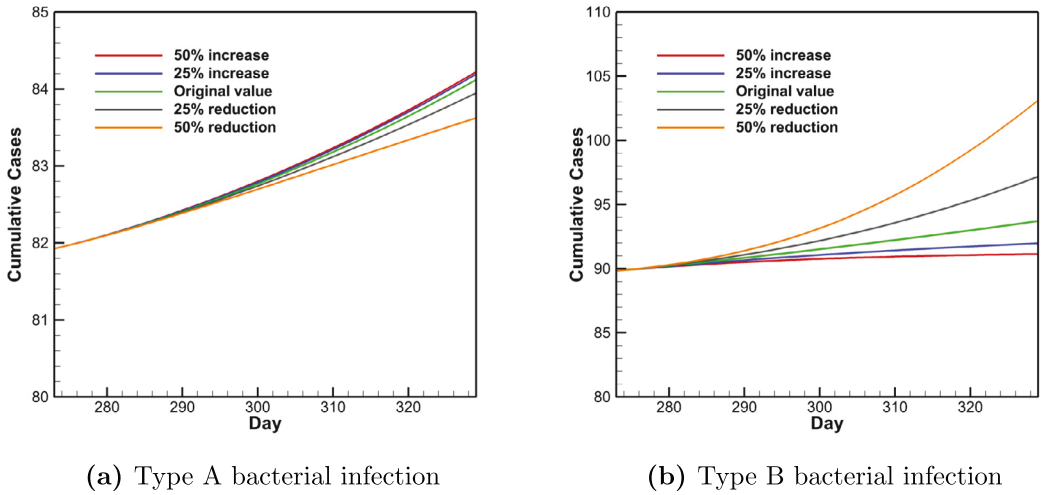

Fig. 11. Model predictions for the number of cumulative cases in an 8-week period (i.e., from day 273 to day 328) immediately following the 272-day fitting period in 2023, with the type B recovery rate γ_1 varied.

the zero-COVID policy in December 2022, the patients' exposure to infectious pathogens, especially resistant bacteria, may have been substantially increased which led to a larger number of cases and higher risk of infection that is measured by the basic reproduction number $\mathscr{R}_0$; see Eq. (3.2). This trend is reflected in our model fitting. In contrast, the infection-induced mortality rate ω fitted in 2022 is higher than that fitted in 2023, possibly due to the comorbidity that was more common in the pandemic era (e.g., patients with both COVID-19 and bacterial infections) and that could lead to more deaths in the ICU.

We have also conducted a series of simulation studies for the 2022 data, and the detailed simulation results are presented in Appendix C. Comparing the results between 2023 and 2023, we observe qualitatively very similar patterns, indicating that the dynamical properties and transmission mechanisms from our deterministic model apply to both years. On the other hand, a small difference is that the variation of β_{01} for 2022 has a slightly larger impact than that for 2023 on the number of cumulative cases (compare Figs. C.6 and 9). This is consistent with the fact that the fitted co-infection rate β_{01} in 2022 has a higher value than its counterpart in 2023 (compare Table 3 and Table 2). As discussed before, though, the co-infection rate plays a relatively minor role in the overall epidemic progression.

4. Discussion

We have formulated a mathematical model to investigate nosocomial infections that are caused by antibiotic sensitive and resistant bacteria. The focus is the presence of multiple transmission routes and their interplay with each other in the process of

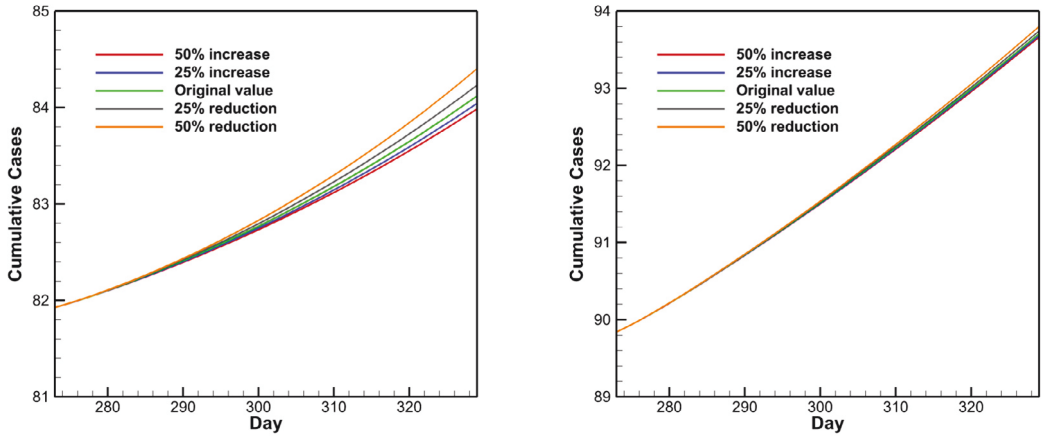

(a) Type A bacterial infection (b) Type B bacterial infection

Fig. 12. Model predictions for the number of cumulative cases in an 8-week period (i.e., from day 273 to day 328) immediately following the 272-day fitting period in 2023, with the co-infection recovery rate γ_{01} varied.

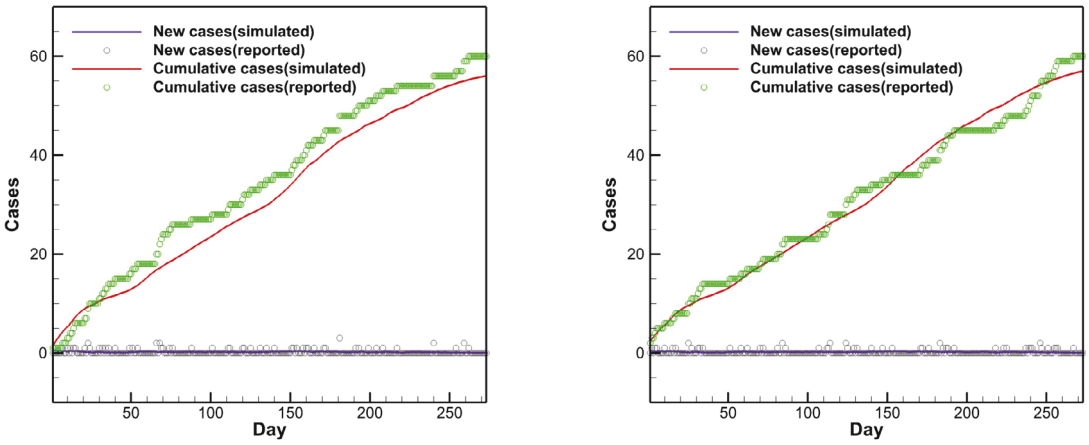

(a) Type A bacterial infection (b) Type B bacterial infection

Fig. 13. Numerical results for the number of new cases and the number of cumulative cases based on the 272-day data in 2022.

disease spread. Our model has incorporated different transmission modes including primary infection, co-infection, and re-infection for each type of bacteria. Using clinical data collected from the ICU of FHUSTC, we have calibrated our model and conducted a range of simulation studies. In particular, we have compared and quantified the significance of each transmission route in the short-term and long-term epidemic development. Our study emphasizes a holistic understanding of the complex dynamics of nosocomial bacterial infections and a strategic design of control measures taking account of the different roles played by the multiple transmission pathways.

The simulation results generated in this work highlight the importance of effective prevention and intervention for antibiotic-resistant bacteria; i.e., type B bacteria in our model. Such bacteria play a more important role than antibiotic-sensitive (i.e., type A) bacteria in shaping both the short-term and long-term progression of the epidemic, as demonstrated in Section 3.2. Meanwhile, as shown in Section 3.3, changes of the type B infection and recovery rates have more significant impacts than those of the type A infection and recovery rates on the number of cumulative cases in the future. These results quantify and confirm empirical observations from hospitals where resistant bacteria are commonly found to be more difficult to treat and possess higher risk for infection, compared to sensitive bacteria. We have also found, for both types of bacteria, that primary infection and re-infection have a larger impact than co-infection in the overall epidemic development and evolution.

Through our predictive simulation in Section 3.3, we have identified that decreasing the type B transmission rate and increasing the type B recovery rate can effectively reduce the number of infections from both type B and type A bacteria. Practically, it may be easier to reduce the transmission rate of resistant bacteria through improvement of the hygiene and sanitation practices

and educational programs in hospitals, through accurate and efficient screening and identification of new positives, and through necessary quarantine and isolation of infected individuals [32,33]. The effects of some of these control strategies have been demonstrated through our data fitting for the year of 2022 (see Section 3.4). To boost the recovery rate, however, it may require new therapeutic strategies to effectively treat those resistant bacteria. It may even demand novel antibiotic drugs whose development is usually a high-cost, time-consuming process [33]. On the other hand, decreasing the type A transmission rate and increasing the type A recovery rate are effective in the control of type A infections, but not so much for type B infections. Our numerical results show that if the type B (or, type A) transmission rate can be reduced by 25%, then the number of type B (or, type A) cumulative cases would barely increase. Similar effects can be achieved by increasing the respective recovery rates by 25%. We have also found that the improvement made by even stronger control measures (e.g., reducing a transmission rate by 50%, or increasing a recovery rate by 50%) is very minor, sometimes barely noticeable. These results could provide quantitative guidelines for healthcare providers and hospital administrators to properly scale their efforts for nosocomial infection control and epidemic management. The findings also motivate a more detailed investigation into the effects of managing bacterial infections in hospitals and the costs of implementing such control measures, and the best balance between the two, which may be achieved through an optimal control study [34].

A limitation of our fitting and simulation results is that the number of infected individuals reported at FHUSTC ICU has remained relatively low. For such a small epidemic, the stochastic/random effects may play a role, which our deterministic model is unable to reflect. We have partially addressed this issue by using data from two different years (2022 and 2023) and have found that our model calibration and data simulation results exhibit similar patterns, providing evidence that the mechanisms of disease transmission and spread revealed from our deterministic model are applicable to different times. On the other hand, results from 2022 and 2023 fitting and simulation also show some noticeable differences, as discussed in Section 3.4.

This work represents a pilot study for comparing and quantifying multiple transmission routes in the spread of nosocomial bacterial infections. Our model is coarse-grained by considering only two broad types of bacteria (i.e., sensitive and resistant bacteria). This simplification allows us to construct a mathematical model incorporating the primary infection, co-infection, and re-infection from each type of bacteria as well as their detailed interplay with each other, while keeping the total number of parameters relatively low. Consequently, the model is well manageable, easily fitted to real data, and readily implemented for predictive simulation. Based on the results from the current work and the availability of more detailed clinical data, refined models may be developed that take into account multiple bacterial strains in each type of (sensitive and resistant) bacteria and that are applicable to different hospital settings.

CRediT authorship contribution statement

Ziqiang Cheng: Writing – review & editing, Writing – original draft, Visualization, Validation, Methodology, Investigation, Formal analysis. **Hengmin Jia:** Writing – original draft, Validation, Resources, Investigation, Formal analysis, Data curation. **Jian Sun:** Investigation, Data curation. **Yueguo Wang:** Investigation, Data curation. **Shusheng Zhou:** Investigation, Data curation. **Kui Jin:** Writing – original draft, Supervision, Methodology, Investigation, Data curation, Conceptualization. **Mengping Zhang:** Supervision, Methodology, Investigation, Conceptualization. **Jin Wang:** Writing – review & editing, Writing – original draft, Supervision, Methodology, Investigation, Conceptualization.

Declaration of competing interest

The authors declare that they have no known competing financial interests or personal relationships that could have appeared to influence the work reported in this paper.

Data availability

Data will be made available upon request.

Acknowledgments

ZC was partially supported by the National Natural Science Foundation of China under grant numbers 12201169 and 32371555, and the Natural Science Foundation of Anhui Province under grant number 2308085MA09. KJ was partially supported by the Key Research and Development Program in Anhui Province of China under grant number 2022e07020085 and the Natural Science Foundation of Anhui Province under grant number 2208085MH235. MZ was partially supported by the National Natural Science Foundation of China under grant number 12126604 and the R&D project of Pazhou Lab (Huangpu) under grant number 2023K0609. JW was partially supported by the National Science Foundation under grant numbers 1951345 and 2324691. The authors would like to thank the handling editor and the two anonymous reviewers for their valuable comments that have improved the quality of the original manuscript.

Appendix A. Dynamical properties of the autonomous system

In system (2.1), all model parameters except the influx rate Γ are positive constants. If we assume that Γ can also be approximated by a positive constant (such as its average over the time interval of our concern), system (2.1) becomes autonomous and its essential dynamics can be mathematically analyzed.

Basic reproduction number. The basic reproduction number $\mathscr{R}_0$, commonly interpreted as the average number of secondary cases produced by one infected individual in a susceptible population, describes the transmissibility (or, contagiousness) of infectious agents. It is one of the fundamental and widely used metrics in epidemiological studies. We derive $\mathscr{R}_0$ for this model using the next-generation matrix technique [35]. It is straightforward to work out the disease-free equilibrium (DFE) of the system as

$$X^0 = \Big(\frac{\Gamma}{\mu}, 0, 0, 0, 0, 0, 0, 0, 0\Big). \tag{A.1}$$

Let $\mathcal{F}$ be the non-negative matrix representing the generation of new infections and $\mathcal{V}$ the non-singular matrix representing the transfer of individuals between compartments. Using the DFE, we can easily find

$$\mathcal{F} = \begin{pmatrix} \frac{\beta_0\Gamma}{\mu} & 0 & \frac{\beta_0\Gamma}{\mu} & \frac{\beta_0\Gamma}{\mu} & 0 \\ 0 & \frac{\beta_1\Gamma}{\mu} & \frac{\beta_1\Gamma}{\mu} & 0 & \frac{\beta_1\Gamma}{\mu} \\ 0 & 0 & 0 & 0 & 0 \\ 0 & 0 & 0 & 0 & 0 \\ 0 & 0 & 0 & 0 & 0 \end{pmatrix}, \quad \mathcal{V} = \begin{pmatrix} \gamma_0+\omega & 0 & 0 & 0 & 0 \\ 0 & \gamma_1+\omega & 0 & 0 & 0 \\ 0 & 0 & \gamma_{01}+\omega & 0 & 0 \\ 0 & 0 & 0 & \gamma_0+\omega & 0 \\ 0 & 0 & 0 & 0 & \gamma_1+\omega \end{pmatrix}.$$

The basic reproduction number can then be computed as:

$$\mathscr{R}_0 = \rho\big(\mathcal{F}\mathcal{V}^{-1}\big) = \max\big(\mathscr{R}_{00}, \mathscr{R}_{01}\big) = \max\left(\frac{\beta_0\Gamma}{\mu(\gamma_0+\omega)}, \frac{\beta_1\Gamma}{\mu(\gamma_1+\omega)}\right), \tag{A.2}$$

where ρ denotes the spectral radius of the next-generation matrix $\mathcal{F}\mathcal{V}^{-1}$. The basic reproduction number here is the maximum of $\mathscr{R}_{00}$ and $\mathscr{R}_{01}$ which represent the risk of infection associated with type A and type B bacteria, respectively.

Equilibrium solutions. Through direct algebraic manipulations, we find this system has the following equilibria:

- When $\mathscr{R}_0 < 1$ (i.e., $\mathscr{R}_{00} < 1$ and $\mathscr{R}_{01} < 1$), the DFE X^0 is the only equilibrium.
- When $\mathscr{R}_{00} > 1$, there exists a type A boundary equilibrium

$$X^A = \big(S^A, I_0^A, I_1^A, I_{01}^A, \tilde{I}_0^A, \tilde{I}_1^A, R_0^A, R_1^A, R_{01}^A\big) \tag{A.3}$$

  where type B infection is not present, with

$$S^A = \frac{\gamma_0+\omega}{\beta_0}, \quad I_0^A = \frac{\Gamma}{\beta_0 S^A} - \frac{\mu}{\beta_0}, \quad R_0^A = \frac{\gamma_0 I_0^A}{\mu}, \quad I_1^A = I_{01}^A = \tilde{I}_1^A = \tilde{I}_0^A = R_1^A = R_{01}^A = 0.$$

- When $\mathscr{R}_{01} > 1$, there exists a type B boundary equilibrium

$$X^B = \big(S^B, I_0^B, I_1^B, I_{01}^B, \tilde{I}_0^B, \tilde{I}_1^B, R_0^B, R_1^B, R_{01}^B\big) \tag{A.4}$$

  where type A infection is not present, with

$$S^B = \frac{\gamma_1+\omega}{\beta_1}, \quad I_1^B = \frac{\Gamma}{\beta_1 S^B} - \frac{\mu}{\beta_1}, \quad R_1^B = \frac{\gamma_1 I_1^B}{\mu}, \quad I_0^B = I_{01}^B = \tilde{I}_0^B = \tilde{I}_1^B = R_0^B = R_{01}^B = 0.$$

- When $\mathscr{R}_{00} > 1$ and $\mathscr{R}_{01} > 1$, there exists a positive endemic equilibrium:

$$X^* = \big(S^*, I_0^*, I_1^*, I_{01}^*, \tilde{I}_0^*, \tilde{I}_1^*, R_0^*, R_1^*, R_{01}^*\big) > 0. \tag{A.5}$$

The first three statements are straightforward to verify. Using the expressions for $\mathscr{R}_{00}$ and $\mathscr{R}_{01}$ in Eq. (A.2), it is also easy to observe that $I_0^A > 0$ when $\mathscr{R}_{00} > 1$, and $I_1^B > 0$ when $\mathscr{R}_{01} > 1$. Thus, the two boundary equilibria X^A and X^B are both biologically feasible. The proof of the fourth statement, however, involves extremely tedious algebraic manipulations. Instead, we have chosen to numerically demonstrate the results, with details given below.

Using the parameter values presented in Tables 1 and 2 based on the data in 2023, we have numerically calculated all the four equilibria of the system, where $\mathscr{R}_{00} > 1$ and $\mathscr{R}_{01} > 1$ from Eq. (3.2). Keeping four decimal places, these equilibrium points are given by

$$\begin{aligned} X^0 &= (6.8315, 0.0000, 0.0000, 0.0000, 0.0000, 0.0000, 0.0000, 0.0000, 0.0000), \\ X^A &= (6.1716, 0.7829, 0.0000, 0.0000, 0.0000, 0.0000, 0.6524, 0.0000, 0.0000), \\ X^B &= (6.1394, 0.0000, 1.4247, 0.0000, 0.0000, 0.0000, 0.0000, 0.6784, 0.0000), \\ X^* &= (5.3753, 0.8018, 1.5549, 0.0516, 0.1013, 0.1695, 0.5858, 0.6550, 0.1897). \end{aligned} \tag{A.6}$$

We have also found that the positive endemic equilibrium X^* is unique. At the endemic level, $I_1^* = 1.5549 > I_0^* = 0.8018$, and $\tilde{I}_1^* = 0.1695 > \tilde{I}_0^* = 0.1013$, indicating that the primary infection and re-infection caused by the resistant bacteria dominate the long-term disease prevalence.

In parallel with the numerical tests for the impact of different transmission pathways (see Section 3.2), we can remove one transmission route at each time to obtain a reduced autonomous system, and then compute its equilibrium solutions. Through numerical calculations, we have the following statements:

(A1) When $I_0 = 0$, the reduced system has only two equilibria, corresponding to the DFE X^0 and type B boundary equilibrium X^B of the original autonomous system.
(A2) When $I_1 = 0$, the reduced system has only two equilibria, corresponding to the DFE X^0 and type A boundary equilibrium X^A of the original autonomous system.
(A3) When $I_{01} = 0$, the reduced system has four equilibria. The first three correspond to the DFE X_0 and the boundary equilibria X^A and X^B of the original system, and the fourth one is a positive equilibrium given by

$$X^{01} = (5.7576, 0.5085, 1.3027, 0.0524, 0.0864, 0.3818, 0.5762, 0.0848). \tag{A.7}$$

(A4) When $\tilde{I}_0 = 0$, the reduced system has four equilibria. The first three correspond to X_0, X^A and X^B of the original system, and the fourth one is a positive equilibrium given by $(6.0394, 0.1032, 1.4460, 0.0055, 0.0185, 0.0771, 0.6785, 0.0114)$.
(A5) When $\tilde{I}_1 = 0$, the reduced system has four equilibria. The first three correspond to X_0, X^A and X^B of the original system, and the fourth one is a positive equilibrium given by $(5.9631, 0.7929, 0.4000, 0.0118, 0.0230, 0.6399, 0.1711, 0.0248)$.
(A6) When $\tilde{I}_0 = \tilde{I}_1 = 0$, the reduced system has four equilibria. The first three correspond to X_0, X^A and X^B of the original system, and the fourth one is a positive equilibrium given by $(6.0752, 0.2886, 1.0451, 0.0110, 0.2219, 0.4781, 0.0053)$.

These results provide a basis to verify the numerical tests conducted in Section 3.2 regarding the long-term dynamics.

Appendix B. Sensitivity analysis for model parameters

We have conducted a sensitivity analysis for the parameters in system (2.1) to quantify their impact on the model outcomes. We utilize the methodology presented in [36] for computing the relative sensitivity of each parameter with respect to the state variables.

We introduce the notations:

$$\begin{aligned} X &= \left(S, I_0, I_1, I_{01}, \tilde{I}_0, \tilde{I}_1, R_0, R_1, R_{01}\right)^T, \\ \alpha &= \left(\beta_0, \beta_1, \beta_{01}, \omega, \gamma_0, \gamma_1, \gamma_{01}, \mu\right)^T, \end{aligned} \tag{B.1}$$

and

$$F(X,\alpha) = \begin{pmatrix} \Gamma - \beta_0 S(I_0 + \tilde{I}_0 + I_{01}) - \beta_1 S(I_1 + \tilde{I}_1 + I_{01}) - \mu S \\ \beta_0 S(I_0 + \tilde{I}_0 + I_{01}) - \beta_{01} I_0(I_1 + \tilde{I}_1 + I_{01}) - (\gamma_0 + \omega) I_0 \\ \beta_1 S(I_1 + \tilde{I}_1 + I_{01}) - (\gamma_1 + \omega) I_1 \\ \beta_{01} I_0(I_1 + \tilde{I}_1 + I_{01}) - (\gamma_{01} + \omega) I_{01} \\ \beta_0 R_1(I_0 + \tilde{I}_0 + I_{01}) - (\gamma_0 + \omega)\tilde{I}_0 \\ \beta_1 R_0(I_1 + \tilde{I}_1 + I_{01}) - (\gamma_1 + \omega)\tilde{I}_1 \\ \gamma_0 I_0 - \beta_1 R_0(I_1 + \tilde{I}_1 + I_{01}) - \mu R_0 \\ \gamma_1 I_1 - \beta_0 R_1(I_0 + \tilde{I}_0 + I_{01}) - \mu R_1 \\ \gamma_{01} I_{01} + \gamma_0 \tilde{I}_0 + \gamma_1 \tilde{I}_1 - \mu R_{01} \end{pmatrix}. \tag{B.2}$$

Then system (2.1) can be written as the following vector form:

$$\frac{dX}{dt} = F(X,\alpha). \tag{B.3}$$

Let X_i and F_i denote the ith component of X and F, respectively, for $1 \le i \le 9$, and α_j denote the jth component of α for $1 \le j \le 8$. Taking the partial derivative of the ith equation in system (B.3) with respect to α_j, we obtain

$$\frac{d}{dt}\frac{\partial X_i}{\partial \alpha_j} = \frac{\partial F_i}{\partial X} \cdot \frac{\partial X}{\partial \alpha_j} + \frac{\partial F_i}{\partial \alpha_j}, \quad 1 \le i \le 9, \quad 1 \le j \le 8. \tag{B.4}$$

The state variables $X_i(t)$ and sensitivity functions $\frac{\partial X_i}{\partial \alpha_j}(t)$ can be solved by combining Eqs. (B.3) and (B.4). We have applied a fourth-order Runge–Kutta method to solve this combined system in both the fitting periods of 2023 and 2022. The sensitivity of each parameter α_j with respect to the state variables is then defined as its maximum relative sensitivity in terms of all variables X_i:

$$\text{Sensitivity of } \alpha_j = \max_i \left(\max_t \left| \frac{\partial X_i}{\partial \alpha_j}(t) \frac{\alpha_j}{X_i(t)} \right| \right), \qquad 1 \le j \le 8. \tag{B.5}$$

Table B.1
Parameter sensitivities with respect to the state variables based on data in 2023.

	S	I_0	I_1	I_{01}	$\tilde{I}_0$	$\tilde{I}_1$	R_0	R_1	R_{01}	Sensitivity
β_0	2.12E+00	6.28E+00	9.51E−01	6.65E+00	6.49E+00	6.48E+00	6.14E+00	2.22E+00	6.28E+00	6.65E+00
β_1	1.85E+00	1.52E+00	4.75E+00	4.06E+00	5.57E+00	4.53E+00	2.64E+00	4.51E+00	4.43E+00	5.57E+00
β_{01}	1.44E−01	2.99E−01	1.70E−01	1.41E+00	4.57E−01	3.91E−01	2.49E−01	1.45E−01	5.35E−01	1.41E+00
ω	7.66E−02	1.57E−01	1.59E−01	2.81E−01	2.95E−01	2.50E−01	1.20E−01	1.41E−01	2.48E−01	2.95E−01
γ_0	2.03E+00	8.41E+00	7.07E−01	7.46E+00	8.64E+00	6.17E+00	6.64E+00	1.78E+00	6.31E+00	8.64E+00
γ_1	1.91E+00	1.41E+00	6.78E+00	5.39E+00	6.37E+00	6.39E+00	2.44E+00	5.39E+00	5.09E+00	6.78E+00
γ_{01}	2.94E−01	8.85E−01	3.08E−01	3.30E+00	1.12E+00	1.06E+00	7.93E−01	2.33E−01	1.07E+00	3.30E+00
μ	1.84E+00	7.11E+00	5.29E+00	1.04E+01	1.18E+01	1.04E+01	6.97E+00	5.75E+00	1.17E+01	1.18E+01

Table B.2
Parameter sensitivities with respect to the state variables based on data in 2022.

	S	I_0	I_1	I_{01}	$\tilde{I}_0$	$\tilde{I}_1$	R_0	R_1	R_{01}	Sensitivity
β_0	2.81E+00	1.06E+01	3.26E+00	1.38E+01	1.40E+01	1.33E+01	9.94E+00	2.53E+00	1.33E+01	1.40E+01
β_1	1.74E+00	1.67E+00	7.98E+00	8.85E+00	1.02E+01	9.09E+00	1.99E+00	7.65E+00	9.08E+00	1.02E+01
β_{01}	2.54E−01	6.41E−01	6.76E−01	2.32E+00	1.43E+00	1.24E+00	5.51E−01	6.21E−01	1.59E+00	2.32E+00
ω	2.65E−01	7.50E−01	8.72E−01	1.64E+00	1.67E+00	1.54E+00	6.48E−01	8.02E−01	1.56E+00	1.67E+00
γ_0	2.47E+00	1.12E+01	3.32E+00	1.42E+01	1.47E+01	1.26E+01	9.41E+00	2.62E+00	1.30E+01	1.47E+01
γ_1	1.59E+00	1.86E+00	8.97E+00	9.84E+00	1.02E+01	1.04E+01	1.66E+00	7.54E+00	9.40E+00	1.04E+01
γ_{01}	5.54E−01	1.69E+00	1.18E+00	4.25E+00	2.95E+00	2.74E+00	1.52E+00	1.05E+00	2.86E+00	4.25E+00
μ	2.73E+00	1.23E+01	1.12E+01	2.27E+01	2.42E+01	2.24E+01	1.20E+01	1.13E+01	2.36E+01	2.42E+01

Table B.3
Parameter sensitivities with respect to the basic reproduction number based on data in 2023.

	$\mathscr{R}_{00}$	$\mathscr{R}_{01}$	Sensitivity
β_0	1.00E+00	0.00E+00	1.00E+00
β_1	0.00E+00	1.00E+00	1.00E+00
β_{01}	0.00E+00	0.00E+00	0.00E+00
ω	1.14E−02	1.97E−02	1.97E−02
γ_0	9.89E−01	0.00E+00	9.89E−01
γ_1	0.00E+00	9.80E−01	9.80E−01
γ_{01}	0.00E+00	0.00E+00	0.00E+00
μ	1.00E+00	1.00E+00	1.00E+00

Table B.4
Parameter sensitivities with respect to the basic reproduction number based on data in 2022.

	$\mathscr{R}_{00}$	$\mathscr{R}_{01}$	Sensitivity
β_0	1.00E+00	0.00E+00	1.00E+00
β_1	0.00E+00	1.00E+00	1.00E+00
β_{01}	0.00E+00	0.00E+00	0.00E+00
ω	3.77E−02	6.42E−02	6.42E−02
γ_0	9.62E−01	0.00E+00	9.62E−01
γ_1	0.00E+00	9.36E−01	9.36E−01
γ_{01}	0.00E+00	0.00E+00	0.00E+00
μ	1.00E+00	1.00E+00	1.00E+00

The relative sensitivity results based on data in 2023 and 2022 are presented in Tables B.1 and B.2, respectively.

Meanwhile, we have also computed the relative sensitivity of each parameter with respect to the basic reproduction number $\mathscr{R}_0$ of the autonomous system. Using Eq. (A.2) and noting that

$$\begin{aligned}\frac{\partial \mathscr{R}_{00}}{\partial \alpha} &= \left(\frac{\Gamma}{\mu(\gamma_0+\omega)}, 0, 0, -\frac{\beta_0\Gamma}{\mu(\gamma_0+\omega)^2}, -\frac{\beta_0\Gamma}{\mu(\gamma_0+\omega)^2}, 0, 0, -\frac{\beta_0\Gamma}{\mu^2(\gamma_0+\omega)}\right)^T,\\ \frac{\partial \mathscr{R}_{01}}{\partial \alpha} &= \left(0, \frac{\Gamma}{\mu(\gamma_1+\omega)}, 0, -\frac{\beta_1\Gamma}{\mu(\gamma_1+\omega)^2}, 0, -\frac{\beta_1\Gamma}{\mu(\gamma_1+\omega)^2}, 0, -\frac{\beta_1\Gamma}{\mu^2(\gamma_1+\omega)}\right)^T,\end{aligned} \tag{B.6}$$

the relative sensitivities of each parameter α_j in terms of $\mathscr{R}_{00}$ and $\mathscr{R}_{01}$ can then be easily obtained, the maximum of which will give the sensitivity of α_j with respect to $\mathscr{R}_0$, $1 \le j \le 8$. The relative sensitivity results based on data in 2023 and 2022 are presented in Tables B.3 and B.4, respectively.

Appendix C. Simulation results based on data in 2022

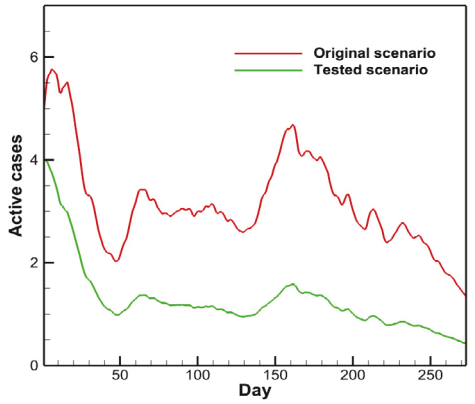

(a) $I_0 = 0$

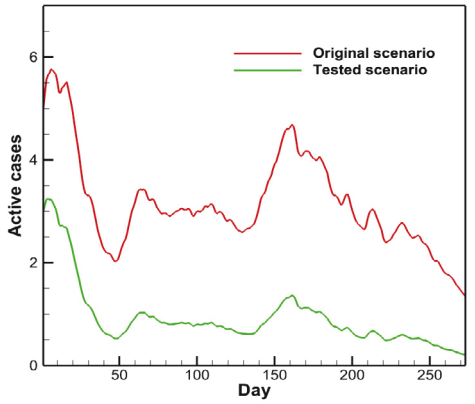

(b) $I_1 = 0$

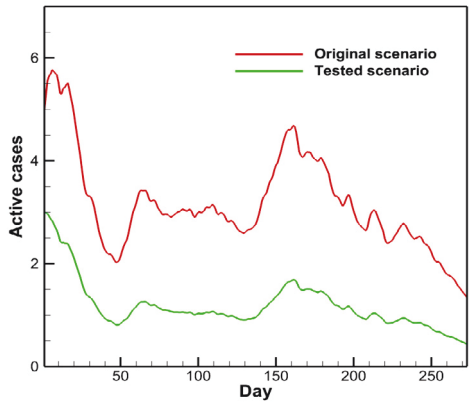

(c) $I_{01} = 0$

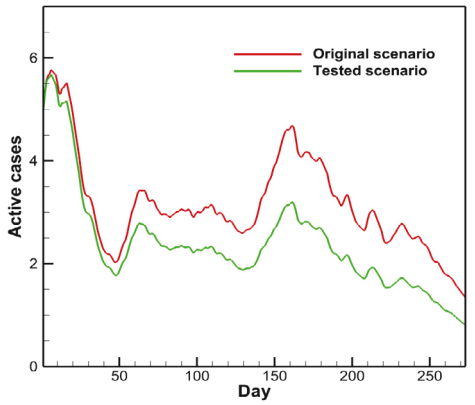

(d) $\tilde{I}_0 = 0$

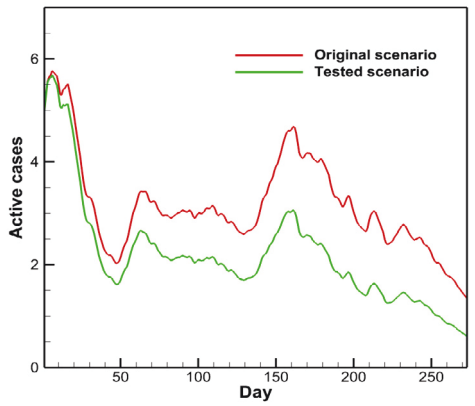

(e) $\tilde{I}_1 = 0$

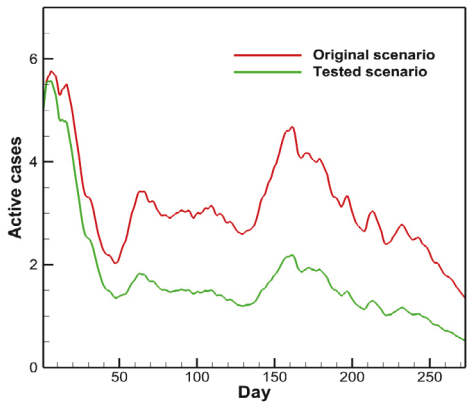

(f) $\tilde{I}_0 = \tilde{I}_1 = 0$

Fig. C.1. Impact of different transmission routes on the number of active cases based on data in 2022.

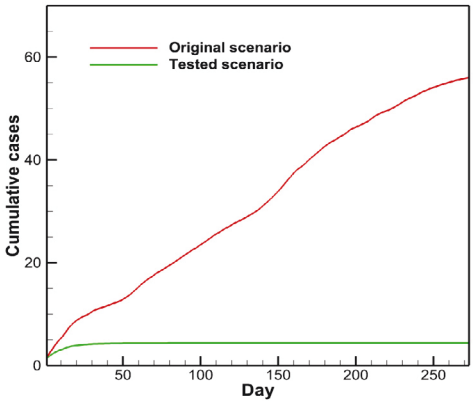

(a) $I_0 = 0$

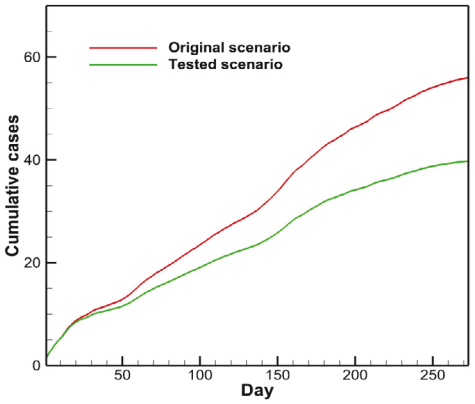

(b) $I_1 = 0$

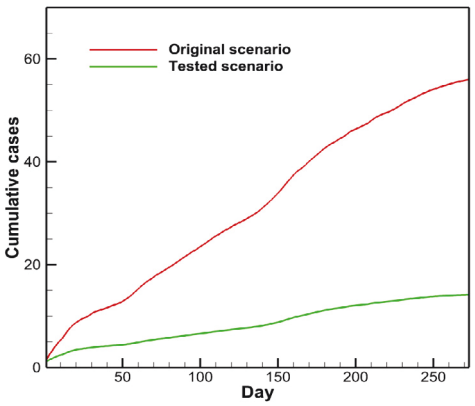

(c) $I_{01} = 0$

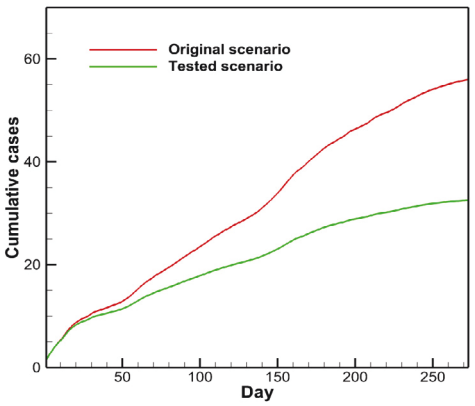

(d) $\tilde{I}_0 = 0$

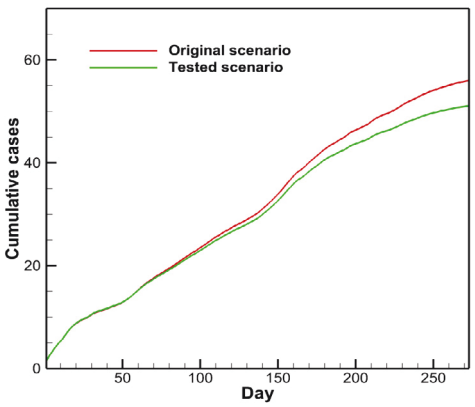

(e) $\tilde{I}_1 = 0$

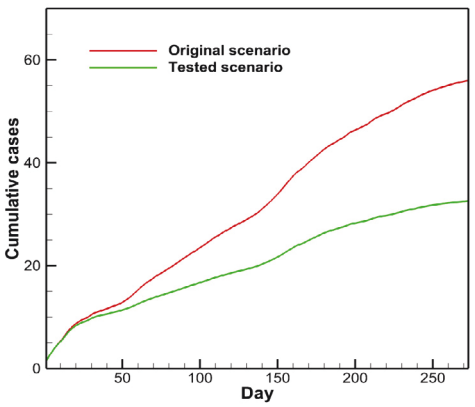

(f) $\tilde{I}_0 = \tilde{I}_1 = 0$

Fig. C.2. Impact of different transmission routes on the number of cumulative cases caused by type A bacteria based on data in 2022.

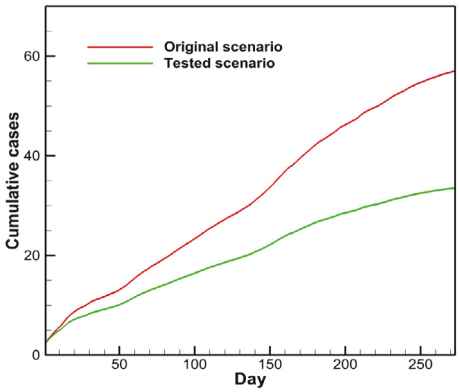

(a) $I_0 = 0$

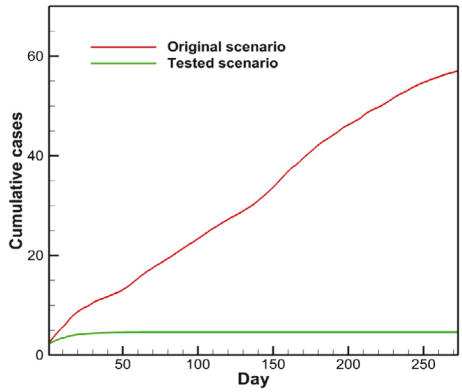

(b) $I_1 = 0$

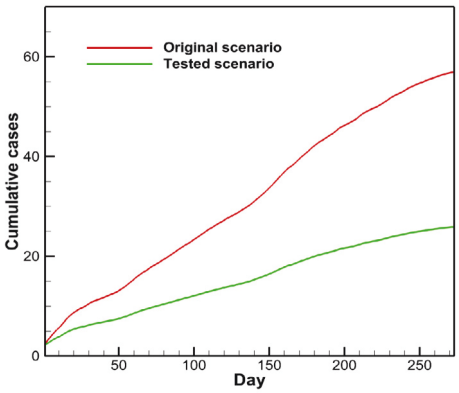

(c) $I_{01} = 0$

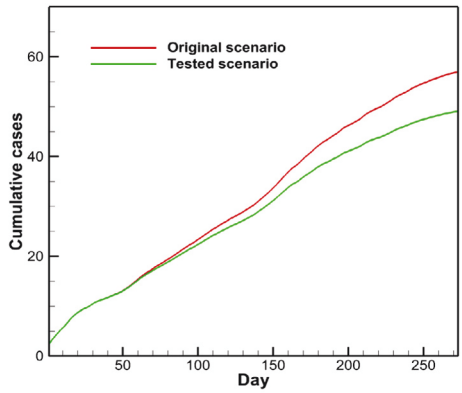

(d) $\tilde{I}_0 = 0$

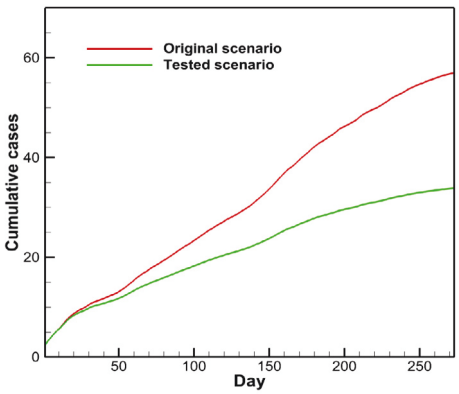

(e) $\tilde{I}_1 = 0$

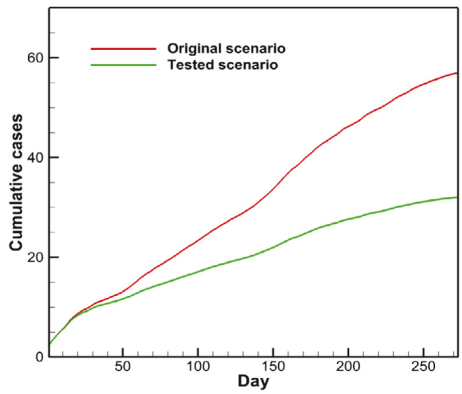

(f) $\tilde{I}_0 = \tilde{I}_1 = 0$

Fig. C.3. Impact of different transmission routes on the number of cumulative cases caused by type B bacteria based on data in 2022.

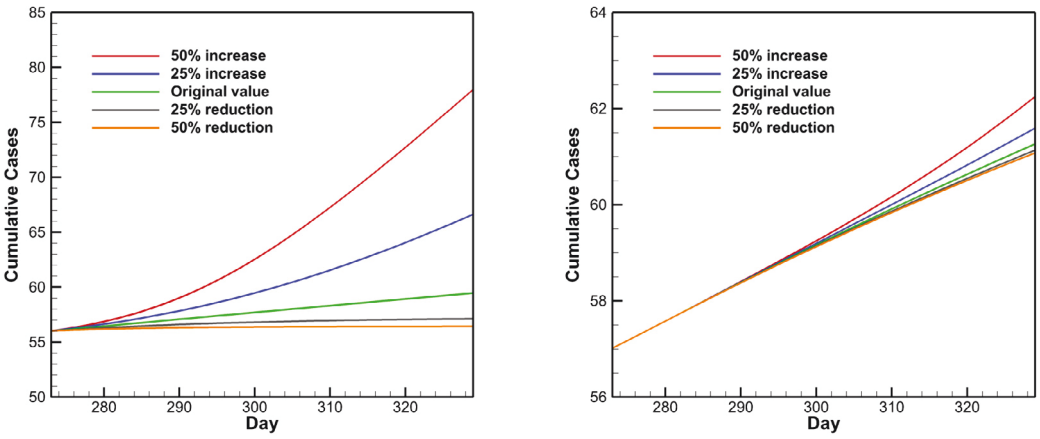

(a) Type A bacterial infection (b) Type B bacterial infection

Fig. C.4. Model predictions for the number of cumulative cases in an 8-week period (i.e., from day 273 to day 328) immediately following the 272-day fitting period in 2022, with the type A transmission rate β_0 varied.

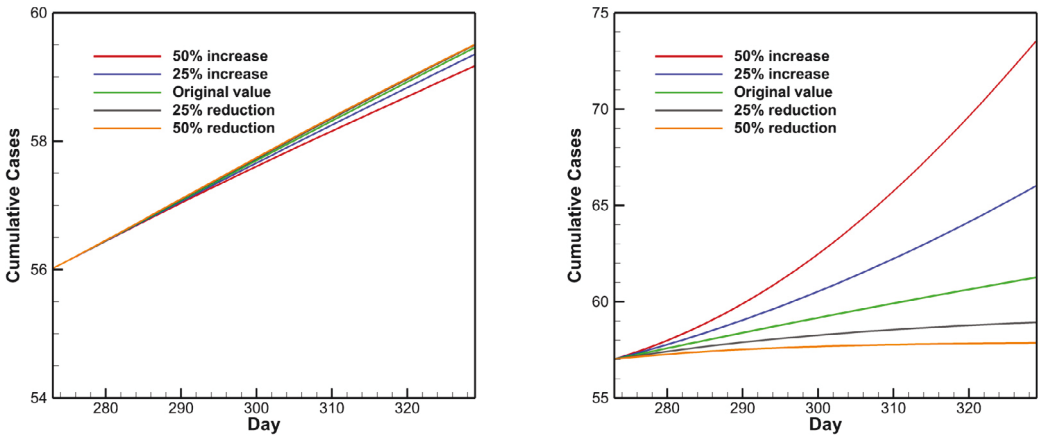

(a) Type A bacterial infection (b) Type B bacterial infection

Fig. C.5. Model predictions for the number of cumulative cases in an 8-week period (i.e., from day 273 to day 328) immediately following the 272-day fitting period in 2022, with the type B transmission rate β_1 varied.

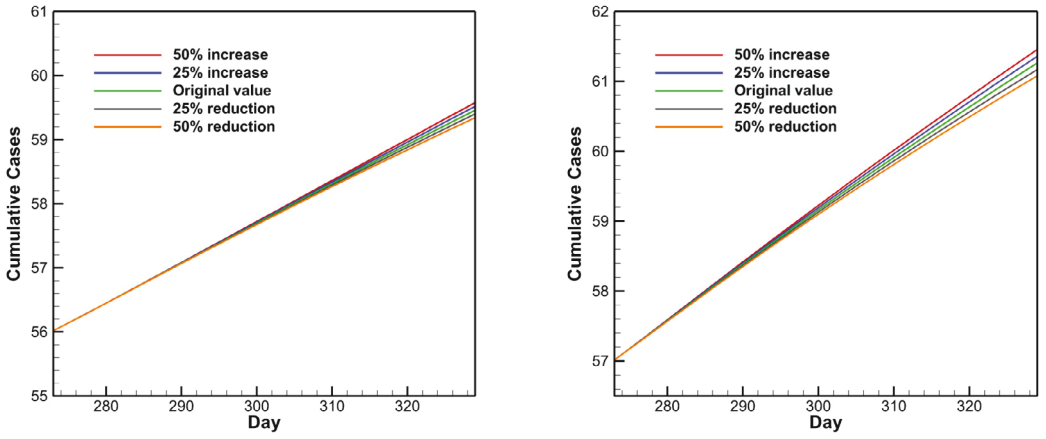

(a) Type A bacterial infection (b) Type B bacterial infection

Fig. C.6. Model predictions for the number of cumulative cases in an 8-week period (i.e., from day 273 to day 328) immediately following the 272-day fitting period in 2022, with the co-infection rate β_{01} varied.

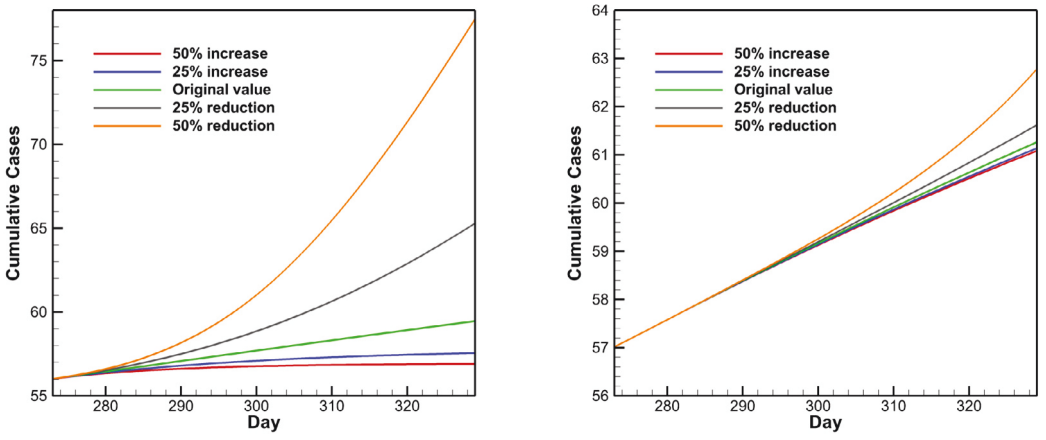

(a) Type A bacterial infection (b) Type B bacterial infection

Fig. C.7. Model predictions for the number of cumulative cases in an 8-week period (i.e., from day 273 to day 328) immediately following the 272-day fitting period in 2022, with the type A recovery rate γ_0 varied.

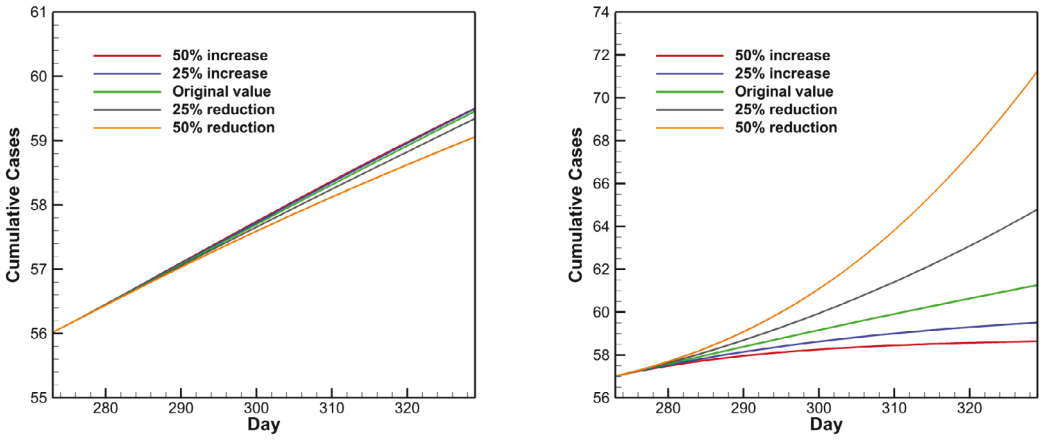

(a) Type A bacterial infection (b) Type B bacterial infection

Fig. C.8. Model predictions for the number of cumulative cases in an 8-week period (i.e., from day 273 to day 328) immediately following the 272-day fitting period in 2022, with the type B recovery rate γ_1 varied.

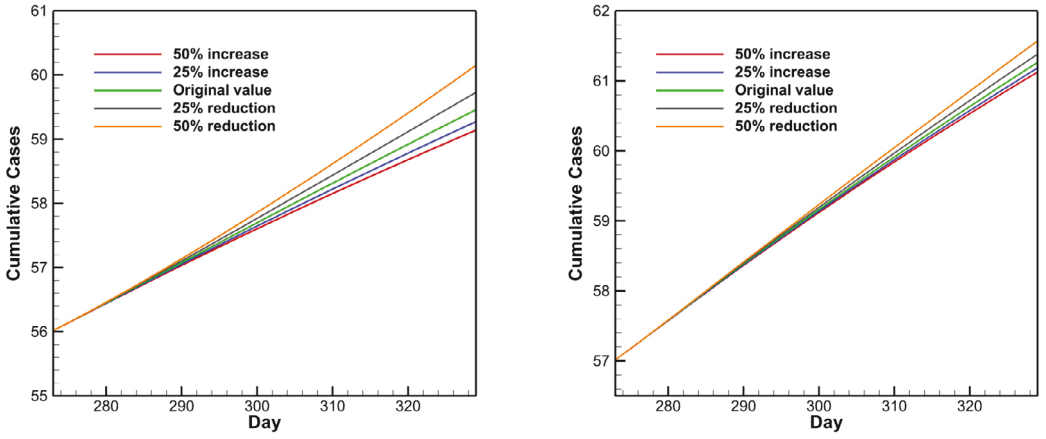

(a) Type A bacterial infection (b) Type B bacterial infection

Fig. C.9. Model predictions for the number of cumulative cases in an 8-week period (i.e., from day 273 to day 328) immediately following the 272-day fitting period in 2022, with the co-infection recovery rate γ_{01} varied.

Here we present our numerical simulation results based on the 2022 data. Figs. C.1–C.3 show the impact of each transmission route on the number of active cases and the number of cumulative cases, corresponding to Figs. 3–5 for the 2023 data. Meanwhile, Figs. C.4–C.9 display the model predictions for the cumulative infections when the three transmission rates and three recovery rates are varied, as analogues to Figs. 7–12 for 2023.

References

[1] Antimicrobial Resistance Collaborators. Global burden of bacterial antimicrobial resistance in 2019: A systematic analysis. Lancet 2022;399(10325):629–55.
[2] Healthcare-associated infections (HAIs). Centers for Disease Control and Prevention, Available at https://www.cdc.gov/hai/index.html.
[3] Review on Antimicrobial Resistance Chaired by Jim O'Neill. Antimicrobial resistance: Tackling a crisis for the health and wealth of nations. 2014, Available at https://amr-review.org/.
[4] Kadri SS. Key takeaways from the U.S. CDC's 2019 antibiotic resistance threats report for frontline providers. Crit Care Med 2020;48(7):939–45.
[5] Antibiotic resistance threats in the United states. Centers for Disease Control and Prevention; 2013, Available at https://www.cdc.gov/drugresistance/pdf/ar-threats-2013-508.pdf.
[6] Laxminarayan R, Matsoso P, Pant S, Brower C, Røttingen JA, Klugman K, Davies S. Access to effective antimicrobials: a worldwide challenge. Lancet 2016;387(10014):168–75.
[7] Knight GM, Davies NG, Colijn C, Coll F, Donker T, Gifford DR, et al. Mathematical modelling for antibiotic resistance control policy: Do we know enough? BMC Infect Dis 2019;19:1011.

[8] Niewiadomska AM, Jayabalasingham B, Seidman JC, Willem L, Grenfell B, Spiro D, Viboud C. Population-level mathematical modeling of antimicrobial resistance: A systematic review. BMC Med 2019;17(1):81.
[9] Spicknall IH, Foxman B, Marrs CF, Eisenberg JN. A modeling framework for the evolution and spread of antibiotic resistance: Literature review and model categorization. Am J Epidemiol 2013;178(4):508–20.
[10] Hethcote HW. The mathematics of infectious diseases. SIAM Rev 2000;42:599–653.
[11] Martcheva M. An introduction to mathematical epidemiology. New York: Springer; 2015.
[12] Lolika PO, Mushayabasa S, Bhunu CP, Modnak C, Wang J. Modeling and analyzing the effects of seasonality on brucellosis infection. Chaos Solitons Fractals 2017;104:338–49.
[13] Wang J. Mathematical models for cholera dynamics–A review. Microorganisms 2022;10(12):2358.
[14] Zhao XQ. Dynamical systems in population biology. Cham: Springer; 2017.
[15] Austin DJ, Anderson RM. Studies of antibiotic resistance within the patient, hospitals and the community using simple mathematical models. Phil Trans R Soc B 1999;354(1384):721–38.
[16] Techitnutsarut P, Chamchod F. Modeling bacterial resistance to antibiotics: Bacterial conjugation and drug effects. Adv Difference Equ 2021;2021:290.
[17] Webb GF, D'Agata EM, Magal P, Ruan S. A model of antibiotic-resistant bacterial epidemics in hospitals. Proc Natl Acad Sci 2005;102(37):13343–8.
[18] D'Agata EM, Magal P, Olivier D, Ruan S, Webb GF. Modeling antibiotic resistance in hospitals: the impact of minimizing treatment duration. J Theoret Biol 2007;249(3):487–99.
[19] Austin DJ, Bonten MJM, Weinstein RA, Slaughter S, Anderson RM. Vancomycin-resistant enterococci in intensive-care hospital settings: transmission dynamics, persistence, and the impact of infection control programs. Proc Natl Acad Sci 1999;96(12):6908–13.
[20] Cooper BS, Medley GF, Scott GM. Preliminary analysis of the transmission dynamics of nosocomial infections: stochastic and management effects. J Hosp Infect 1999;43(2):131–47.
[21] McBryde ES, Pettitt AN, McElwain DLS. A stochastic mathematical model of methicillin resistant staphylococcus aureus transmission in an intensive care unit: predicting the impact of interventions. J Theoret Biol 2007;245(3):470–81.
[22] Wang X, Xiao Y, Wang J, Lu X. Stochastic disease dynamics of a hospital infection model. Math Biosci 2013;241(1):115–24.
[23] Durham LK, Ge M, Cuccia AJ, Quinn JP. Modeling antibiotic resistance to project future rates: Quinolone resistance in Escherichia coli. Eur J Clin Microbiol Infect Dis 2010;29(3):353–6.
[24] Limaye SS, Mastrangelo CM, Zerr DM, Jeffries H. A statistical approach to reduce hospital-associated infections. Qual Eng 2008;20(4):414–25.
[25] Benneyan JC. Statistical quality control methods in infection control and hospital epidemiology, part I: introduction and basic theory. Infect Control Hos Epidemiol 1998;19(3):194–214.
[26] Birnbaum D, Benneyan JC. Statistical quality control methods in infection control and hospital epidemiology, part II: chart use, statistical properties, and research issues. Infect Control Hosp Epidemiol 1998;19(4):265–83.
[27] Cooper B, Lipsitch M. The analysis of hospital infection data using hidden Markov models. Biostatistics 2004;5(2):223–37.
[28] Lin MY, Lyles-Banks RD, Lolans K, Hines DW, Spear JB, Petrak R, Trick WE, Weinstein RA, Hayden MK. Centers for disease control, and prevention epicenters program. The importance of long-term acute care hospitals in the regional epidemiology of Klebsiella pneumoniae carbapenemase-producing Enterobacteriaceae. Clin Infect Dis 2013;57(9):1246–52.
[29] Rafa E, Wałaszek MZ, Wałaszek MJ, Domański A, Rózańska A. The incidence of healthcare-associated infections, their clinical forms, and microbiological agents in intensive care units in Southern Poland in a multicentre study from 2016 to 2019. Int J Environ Res Public Health 2021;18(5):2238.
[30] Vincent JL, Sakr Y, Singer M, Martin-Loeches I, Machado FR, Marshall JC, Finfer S, Pelosi P, Brazzi L, Aditianingsih D, et al. Prevalence and outcomes of infection among patients in Intensive Care Units in 2017. J Am Med Assoc 2020;323(15):1478–87.
[31] Ba Z, Li Y, Ma J, Qin Y, Tian J, Meng Y, Yi J, Zhang Y, Chen F. Reflections on the dynamic zero-COVID policy in China. Prev Med Rep 2023;36:102466.
[32] Antimicrobial resistance. Centers for Disease Control and Prevention, Available at https://www.cdc.gov/drugresistance/index.html.
[33] Metz M, Shlaes DM. Eight more ways to deal with antibiotic resistance. Antimicrob Agents Chemother 2014;58(8):4253–6.
[34] Lenhart S, Workman JT. Workman optimal control applied to biological models. Boca Raton: Chapman Hall/CRC; 2007.
[35] van den Driessche P, Watmough J. Reproduction numbers and sub-threshold endemic equilibria for compartmental models of disease transmission. Math Biosci 2002;180(1–2):29–48.
[36] Ellwein LM, Tran HT, Zapata C, Novak V, Olufsen MS. Sensitivity analysis and model assessment: mathematical models for arterial blood flow and blood pressure. Cardiovasc Eng 2008;8:94–108.